

This is a repository copy of *Seven indicators variations for multiple PV array configurations under partial shading and faulty PV conditions*.

White Rose Research Online URL for this paper:

<https://eprints.whiterose.ac.uk/177675/>

Version: Accepted Version

---

**Article:**

Dhimish, Mahmoud, Holmes, Violeta, Mehrdadi, Bruce et al. (3 more authors) (2017) Seven indicators variations for multiple PV array configurations under partial shading and faulty PV conditions. *Renewable Energy*. pp. 438-460. ISSN 0960-1481

<https://doi.org/10.1016/j.renene.2017.06.014>

---

**Reuse**

Items deposited in White Rose Research Online are protected by copyright, with all rights reserved unless indicated otherwise. They may be downloaded and/or printed for private study, or other acts as permitted by national copyright laws. The publisher or other rights holders may allow further reproduction and re-use of the full text version. This is indicated by the licence information on the White Rose Research Online record for the item.

**Takedown**

If you consider content in White Rose Research Online to be in breach of UK law, please notify us by emailing [eprints@whiterose.ac.uk](mailto:eprints@whiterose.ac.uk) including the URL of the record and the reason for the withdrawal request.

# Seven indicators variations for multiple PV array configurations under partial shading and faulty PV conditions

Mahmoud Dhimish<sup>1</sup>, Violeta Holmes<sup>1</sup>, Bruce Mehrdadi<sup>1</sup>, Mark Dales<sup>1</sup>, Benjamin Chong<sup>2</sup>, Li Zhang<sup>2</sup>

<sup>1</sup> School of Computing and Engineering, University of Huddersfield, United Kingdom

<sup>2</sup> School of Electronic and Electrical Engineering, University of Leeds, United Kingdom

---

## Abstract

The goal of this paper is to model, compare and analyze the performance of multiple photovoltaic (PV) array configurations under various partial shading and faulty PV conditions. For this purpose, a multiple PV array configurations including series (S), parallel (P), series-parallel (SP), total-cross-tied (TCT) and bridge-linked (BL) are carried out under several partial shading conditions such as, increase or decrease in the partial shading on a row of PV modules and increase or decrease in the partial shading on a column of PV modules. Additionally, in order to test the performance of each PV configuration under faulty PV conditions, from 1 to 6 Faulty PV modules have been disconnected in each PV array configuration. Several indicators such as short circuit current ( $I_{sc}$ ), current at maximum power point ( $I_{mpp}$ ), open circuit voltage ( $V_{oc}$ ), voltage at maximum power point ( $V_{mpp}$ ), series resistance ( $R_s$ ), fill factor (FF) and thermal voltage ( $V_{te}$ ) have been used to compare the obtained results from each partial shading and PV faulty condition applied to the PV system. MATLAB/Simulink software is used to perform the simulation and the analysis for each examined PV array configuration.

**Keywords:** Multiple PV array configurations, Partial shading, Fault detection, MATLAB/Simulink

---

## 1. Introduction

Growing interest in renewable energy resources has caused the photovoltaic (PV) power market to expand rapidly. The power produced by grid-connected photovoltaic (GCPV) plants depends on various conditions such as PV module's temperature and irradiance level. Shading by the surroundings directly effects both the cell temperature and irradiance level incident on the GCPV systems [1]. There are multiple reasons for the shading affects GCPV systems. K. Lappalainen & S. Valkealahti [2] discussed the output power variations of different PV array configurations during irradiance transition caused by moving cloud. The results shows that the average rate of change in the output power during irradiance transitions is around 3%, where the maximum rate of change is approximate to 75%. Furthermore, an accurate approach method to simulate the characteristics output of a PV systems under either partial shading or mismatch conditions is proposed by J. Bai et al [3]. The method is using the analysis of the current-voltage (I-V) and power-voltage (P-V) curves for various PV systems.

A highly detailed PV array model is developed by M. Vincenzo et al [4], the PV model was developed under non-uniform irradiance conditions using PSpice. The model assumed that the PV cells temperature are homogenous for each PV module which makes the simulation and modelling of the PV system less complex. The output results shows a good agreement between the simulation model vs. outdoor experimental results. The losses associated to shading effect can be reduced by using several approaches such as the maximum power point tracking (MPPT) techniques that allow the extension of the global maximum power point. R. Yeung et al [5] proposed a global MPPT algorithm which is based on extracting the power-voltage characteristics of the PV string through varying the input power impedance.

42 PV array configurations which is considered in this paper is one of solutions that can significantly reduce  
43 mismatch and shading losses in GCPV plants. It is based on the PV array interconnections of PV modules  
44 which are series (S), parallel (P), series-parallel (SP), total-cross-tied (TCT) and bridge-linked (BL) and  
45 many other configurations. Several attempts were proposed by researchers to study and analyze the effect  
46 of shading on different PV array configuration in order to reduce mismatch losses and providing the  
47 maximum output power generation. These attempts can be illustrated by the following:

48 1. Comparison of various PV array configurations:

49 F. Belhachat & C. Larbes [6] detailed a brief comparison between five different PV array  
50 configurations (S, P, SP, TCT and BL configurations). The analysis is based on  
51 MATLAB/Simulink software. The results prove that TCT configuration achieved the optimum  
52 output power performance under most shading conditions. Moreover, [7] shows a mathematical  
53 analysis of TCT PV array configuration under partial shading conditions and its comparison with  
54 other PV array configurations such as BL and honey-comb (HC) configurations. Y. Wang & P.  
55 Hsu [8] found again that in most cases TCT configuration has a superior performance over the other  
56 PV array configurations such as S, P and SP. Some other publications are based on a comprehensive  
57 review on PV array configuration under partial shading conditions such as [9 & 10].  
58

59 2. New proposed PV array configuration:

60 S. Pareek & R. dahiya [11] proposed a new method that allows the distribution of shading effect  
61 evenly in each PV row thereby enhance the PV array output power. The PV characteristics curves  
62 for the proposed method is much smoother than other PV array configurations such as TCT.  
63 Furthermore, B. Rani et al [12] suggested a new method for increasing the power generation from  
64 PV array configuration. In the proposed approach, the physical location of the PV modules are  
65 connected using TCT configuration, but all PV arrays are arranged based on “Su Do Ku” puzzle  
66 pattern. The performance of the system is investigated for different shading patterns and the results  
67 show that positioning the modules of the array according to “Su Do Ku” puzzle pattern yields  
68 improved performance under partially shaded conditions. However, this method faces a drawbacks  
69 due to ineffective dispersion of shade and significant increase in wiring requirements, these  
70 disadvantages of the “Su Do Ku” method have been enhanced using a new technique which is  
71 proposed by S. Potnure et al [13].  
72

73 3. Power electronics techniques for enhancing PV power generation:

74 B. Chong & L. Zhang [14] proposed a new controller design for integrated PV-converter modules  
75 under partial shading conditions. The control results showing rapid and stable responses are  
76 superior to that obtained by bypass diode structure which is conventionally controlled using  
77 perturbation-and-observation method. Furthermore, a new GCPV based on cascaded H-Bridge  
78 quasi-z source inverter is presented by [15], the technique is used to verify the multilevel PV  
79 interface with AC inverters to enhance the power generation of GCPV systems. E. Koutroulis & F.  
80 Blaabjerg [16] proposed a new procedure for tracking the global maximum power point of PV  
81 arrays operating under partial shading conditions using D-flip/flop and analog/digital converter  
82 strategy. Additionally, a brief comprehensive maximum power point extraction using genetic  
83 algorithm is shown in [17].  
84

85 4. PV fault detection algorithms:

86 There are various methods used to detect faults in GCPV plants. Some of these methods use  
87 statistical analysis techniques such as t-test [18 & 19] and standard deviation limits [20].

88 Furthermore, machine learning techniques have been also applied in PV systems for fault detection  
 89 purposes. ANN network was used by [21] for detection multiple faults in a PV system such as  
 90 faulty PV modules and faulty bypass diodes. S. Silvestre et al [22] proposed a new procedure for  
 91 fault detection in PV systems which is based on the analysis of the voltage and current ratios for  
 92 the entire GCPV plant.

93 In this work, we present a detailed modelling, comparison and data analysis for multiple PV array  
 94 configurations including the series (S), parallel (P), series-parallel (SP), total-cross-tied (TCT) and bridge-  
 95 linked (BL) configurations. In order to compare the performance for each PV array configuration, various  
 96 partial shading and faulty PV conditions have been tested. Several indicators such as short circuit current  
 97 ( $I_{sc}$ ), current at maximum power point ( $I_{mpp}$ ), open circuit voltage ( $V_{oc}$ ), voltage at maximum power point  
 98 ( $V_{mpp}$ ), series resistance ( $R_s$ ), fill factor (FF) and thermal voltage ( $V_{te}$ ) have been used to compare the  
 99 obtained by the tested partial shading and faulty conditions.

100 Fig. 1 shows the overall examined PV array configurations, tested case scenarios and all indicators used to  
 101 compare the performance between each PV array configuration. As can be noticed, the partial shading  
 102 conditions applied in this paper is not static, which means that the partial shading conditions are either  
 103 increasing or decreasing among all PV modules. Additionally, in order to test the performance of each PV  
 104 array configuration under faulty PV conditions, from 1 to 6 Faulty PV modules have been disconnected in  
 105 order to compare between each PV indicator variations.

106 From the literature, there is a few data analysis on the indicators variations among partial shading and faulty  
 107 PV conditions applied to multiple PV array configurations, therefore, the main contribution of this article  
 108 is the comparison and data analysis of multiple PV array configurations using seven different indicators.  
 109 The examined indicators has not been fully covered in previously published articles such as [6-10].  
 110 Additionally, this research does not only examine several partial shading conditions affecting PV systems  
 111 but also the modelling and the analysis of several faulty PV conditions (In-active PV modules) affecting  
 112 various PV array configurations.

113 This paper is organized as follows: Section 2 presents the modelling and simulation for one PV module  
 114 using MATLAB/Simulink software. Section 3 describes the calculation of the diagnostic indicators, while  
 115 section 4 illustrates the simulation, modelling and data analysis of the examined PV array configurations.  
 116 Finally, section 5 and section 6 describes the discussion and the conclusion respectively.

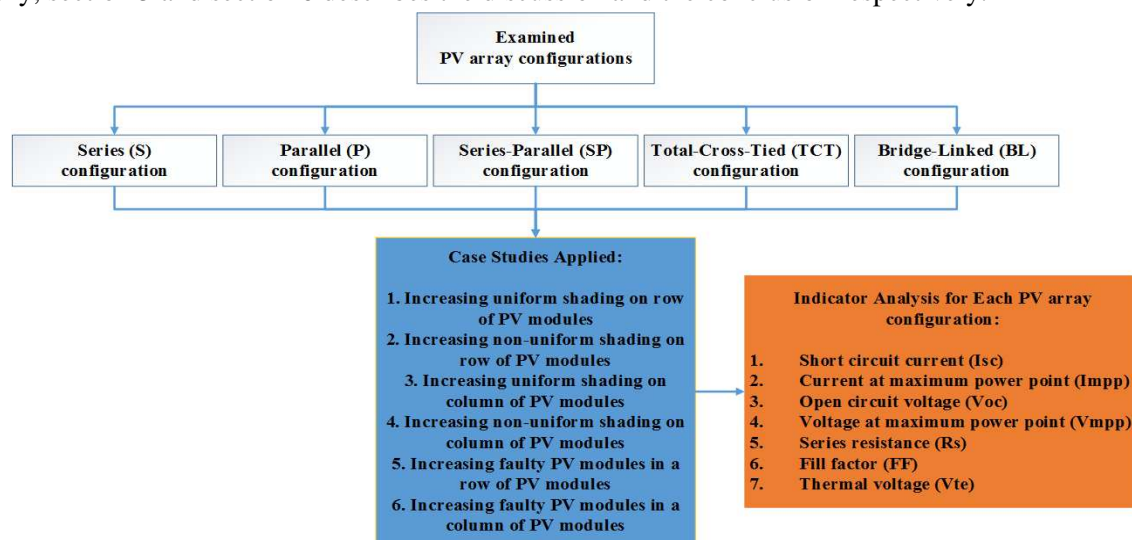


Fig. 1. All Listed PV Array Configurations Compared in this Paper, Tested Case Studies and All Indicators Used to Compare the Performance of Each PV Array Configuration

117 **2. Modelling and simulation of one PV module**

118 In this work, MATLAB/Simulink software is used to model, simulate and analyze the performance of the  
 119 examined PV modules. Fig. 3(a) shows the equivalent circuit of a PV module. The voltage and the current  
 120 characteristics of the PV module can be obtained using the single diode model [23] as explained in (1).

121 
$$I = I_{ph} - I_o \left( e^{\frac{V+IR_s}{N_s V_t}} - 1 \right) - \left( \frac{V+IR_s}{R_{sh}} \right) \quad (1)$$

122 where  $I_{ph}$  is the photo-generated current at STC,  $I_o$  is the dark saturation current at STC,  $R_s$  is the module  
 123 series resistance,  $R_{sh}$  is the panel parallel resistance,  $N_s$  is the number of series cells in the PV module and  
 124  $V_t$  is the thermal voltage and it can be calculated using (2).

125 
$$V_t = \frac{A k T}{q} \quad (2)$$

126 where  $A$  the diode ideality factor,  $k$  is Boltzmann’s constant,  $T$  is the module temperature in kelvin and  $q$   
 127 is the charge of the electron.

128 The five parameters model are determined by solving the transcendental equation (1) using Newton-  
 129 Raphson algorithm [24] based only on the datasheet of the available parameters shown in Table I. The  
 130 power produced by PV module in watts can be easily calculated along with the current (I) and voltage (V)  
 131 that is generated by equation (1), therefore,  $P_{\text{theoretical}} = IV$ .

132 Fig 3(b) shows the PV module simulated at standard test conditions (STC):

- 133
  - Irradiance 1000 W/m<sup>2</sup>, spectrum AM 1.5 G
  - 134 • PV module temperature 25 °C

135 Using the MATLAB/Simulink software, it is possible to simulate the output voltage, current and the power  
 136 of the PV module as shown in Fig. 3(c). As an example of simulation, Fig 2(a) and Fig2(b) show  
 137 respectively the I-V and P-V curves of one PV module of 60 solar cells obtained with Simulink using the  
 138 model described in Fig. 3(c). In this paper, the solar cell parameters used in the simulation are shown in  
 139 Table1.

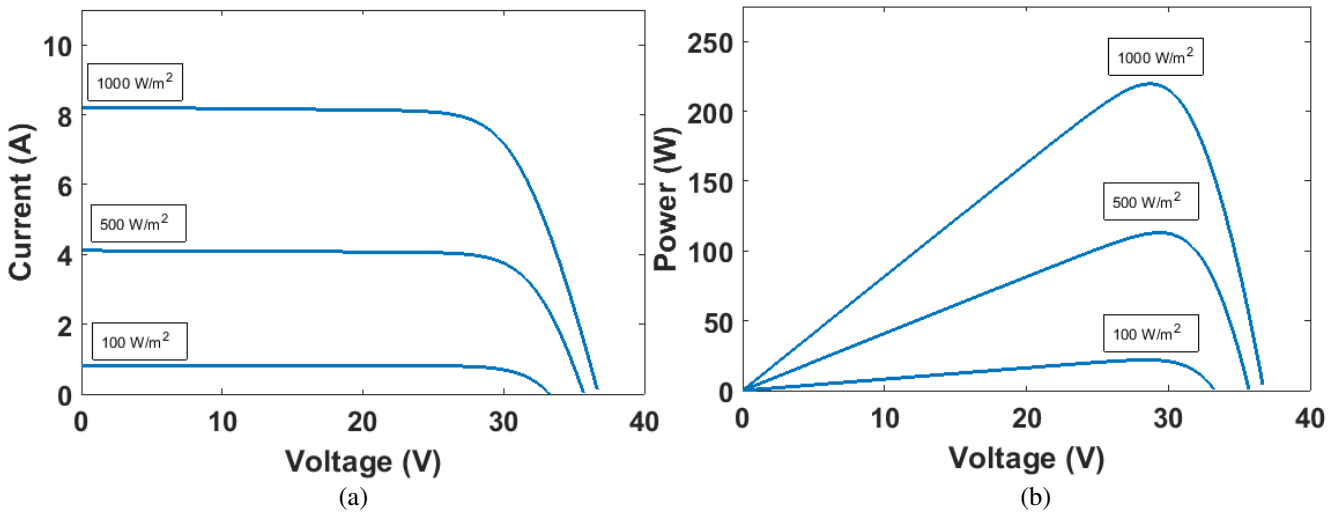


Fig. 2. Simulation Results of MALTBAL/Simulink model. (a) Photovoltaic I-V Curve, (b) Photovoltaic P-V Curve

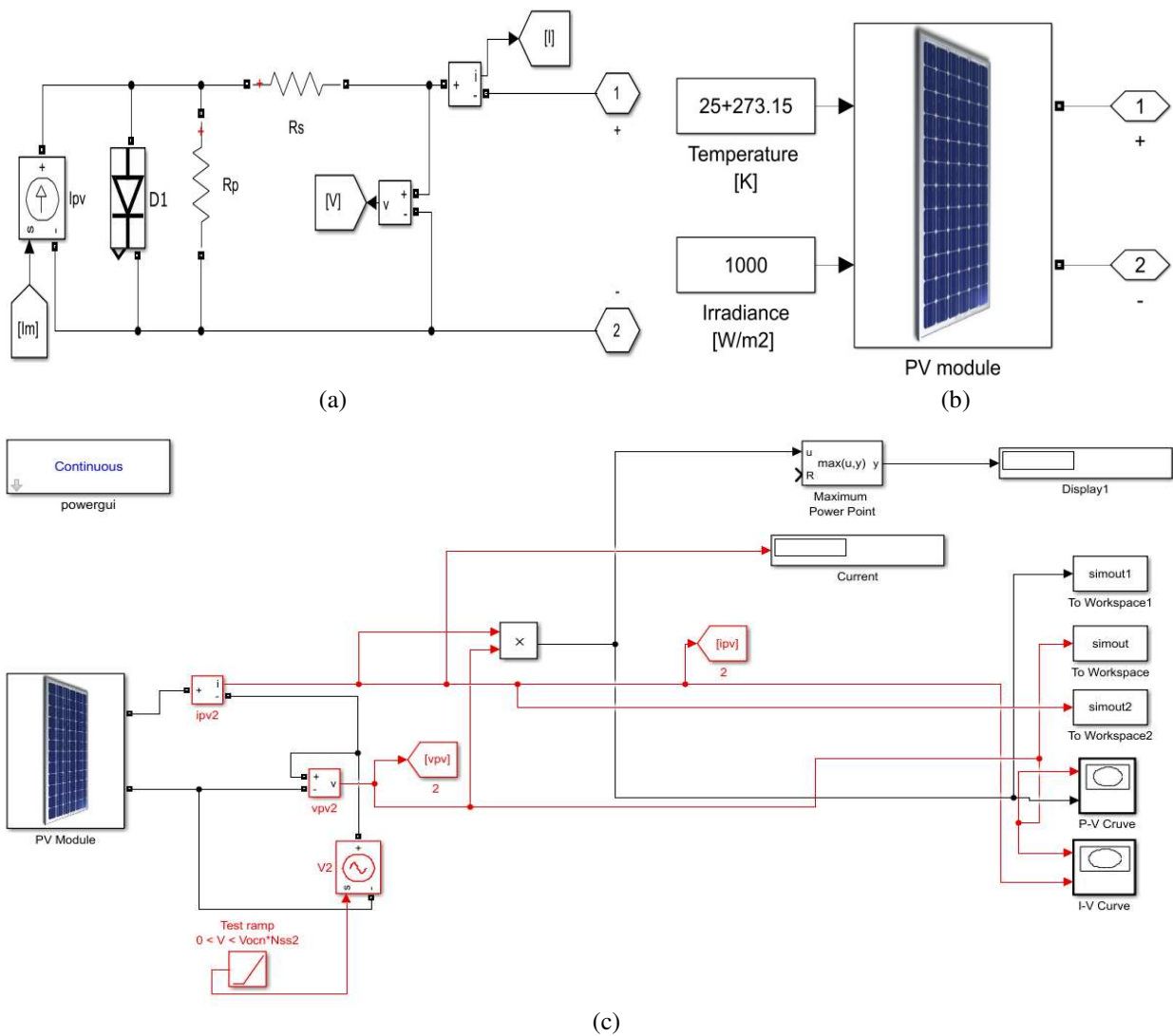


Fig. 3. Photovoltaic Modelling Using MATLAB/Simulink. (a) Equivalent Circuit of a Solar Module, (b) Simulating PV Module under STC, (c) Simulating the Output Voltage, Current and Power of the PV Module

Table 1  
Electrical characteristics of SMT (60) P PV module

Solar panel electrical characteristics	Value
Peak power	220 W
Voltage at maximum power point ( $V_{mp}$ )	28.7 V
Current at maximum power point ( $I_{mp}$ )	7.67 A
Open circuit voltage ( $V_{oc}$ )	36.74 V
Short circuit current ( $I_{sc}$ )	8.24 A
Number of cells connected in series	60
Number of cells connected in parallel	1
Series resistance ( $R_s$ )	0.48484 $\Omega$
Parallel resistance ( $R_{sh}$ )	258.75 $\Omega$
Dark saturation current ( $I_0$ )	$2.8 \times 10^{-10}$ A
Ideal diode factor (A)	0.9117
Boltzmann's constant (k)	$1.3806 \times 10^{-23}$ J.K <sup>-1</sup>

140 **3. Calculation of the diagnostic indicators**

141 In order to compare the behavior of various PV array configurations. Firstly, it is required to identify the  
142 main indicators needed to investigate the change of the PV array configurations behavior. In this paper, a  
143 comparison between  $V_{mpp}$ ,  $V_{oc}$ ,  $I_{mpp}$ ,  $I_{sc}$  and  $P_{mpp}$  have been estimated for various PV array configurations.  
144 Additionally, new diagnostic indicators have been used and briefly explained in this section.

145 **3.1 Equivalent thermal voltage ( $V_{te}$ )**

146 In previous work [25 & 27] an estimation of the thermal voltage of a PV model under partial shading  
147 conditions has been expressed by (3).

148 
$$V_{te} = \frac{(2V_{mp} - V_{oc})(I_{sc} - I_{mp})}{I_{mp} - (I_{sc} - I_{mp}) \ln\left(\frac{I_{sc} - I_{mp}}{I_{sc}}\right)} \quad (3)$$

149 where  $V_{mp}$  is voltage at maximum power point,  $I_{mp}$  presents the current at the maximum power point,  $V_{oc}$  is  
150 the open circuit voltage and  $I_{sc}$  is the short circuit current estimated by the I-V or P-V curve of the PV  
151 module.

152 A second commonly used method to estimate the thermal voltage is to evaluate the change of the diode  
153 ideality factor  $A$  of the PV module [26]. This method can be calculated using (4).

154 
$$V_{te} = \frac{N_s A k T}{q} \quad (4)$$

155 where  $N_s$  is the number of solar cells connected in series,  $k$  is the Boltzmann constant,  $T$  is the junction  
156 temperature in kelvin and  $q$  is equal to the charge of an electron.

157 In this paper, the first method was used to estimate the thermal voltage due to its simplicity and it does not  
158 require the estimation of the ideality factor for the PV modules [18]. The estimation of the ideality factor is  
159 usually cannot be calculated using the maximum power point tracking units provided in the PV systems.  
160 However, the first method does contain all parameters which are normally available to the user of the grid-  
161 connected PV (GCPV) plants.

162 The estimation of  $V_{te}$  for the PV module used in this paper under various irradiance levels (100~1000 W/m<sup>2</sup>)  
163 are shown in Fig. 4. The PV module temperature for all measurements is at STC 25 °C and the solar cell  
164 parameters used in the simulation are shown in Table1.

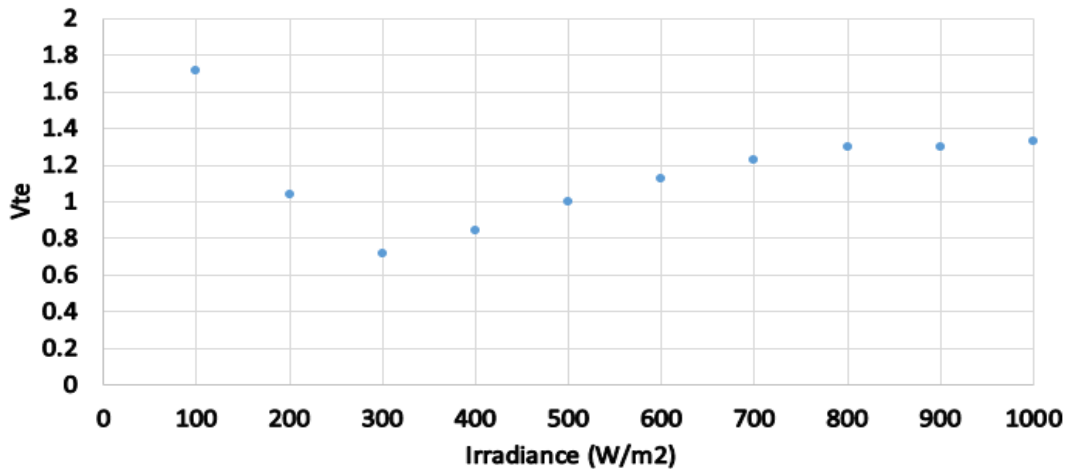


Fig. 4. Thermal Voltage Estimation under Various Irradiance Levels

165 **3.2 Fill factor (FF)**

166 The fill factor (FF) is a generic diagnostic indicator which is sensitive to power losses due to shading and  
 167 faulty conditions occurring in PV systems [27]. FF is sufficiently robust to the irradiance change and the  
 168 temperature levels. FF can be calculated using (5).

169 
$$FF = \frac{I_{mp} V_{mp}}{I_{sc} V_{oc}} \tag{5}$$

170 The fill factor is a good indicator since it depends on the voltage and current changes in the PV modules.  
 171 Fig. 5(a) shows the I-V curve of the PV module used in this work. Also it shows the location of the  
 172 parameters used in the calculation of the FF indicator.

173 At STC, the PV module used in this work can be evaluated as shown in (6).

174 
$$FF = \frac{I_{mp} V_{mp}}{I_{sc} V_{oc}} = \frac{7.67 \times 28.7}{8.18 \times 36.74} = 73.25\% \tag{6}$$

175 Fig. 5(b) shows the variations of the FF under various irradiance levels (100~1000 W/m<sup>2</sup>).

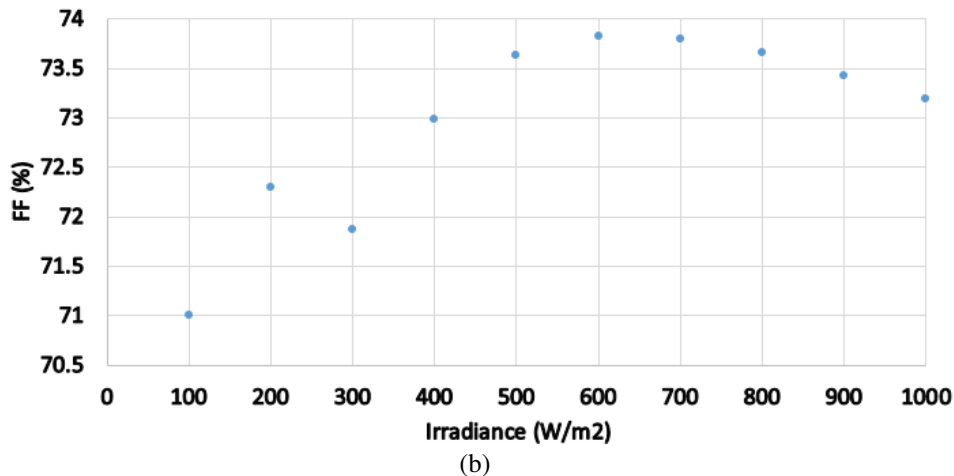
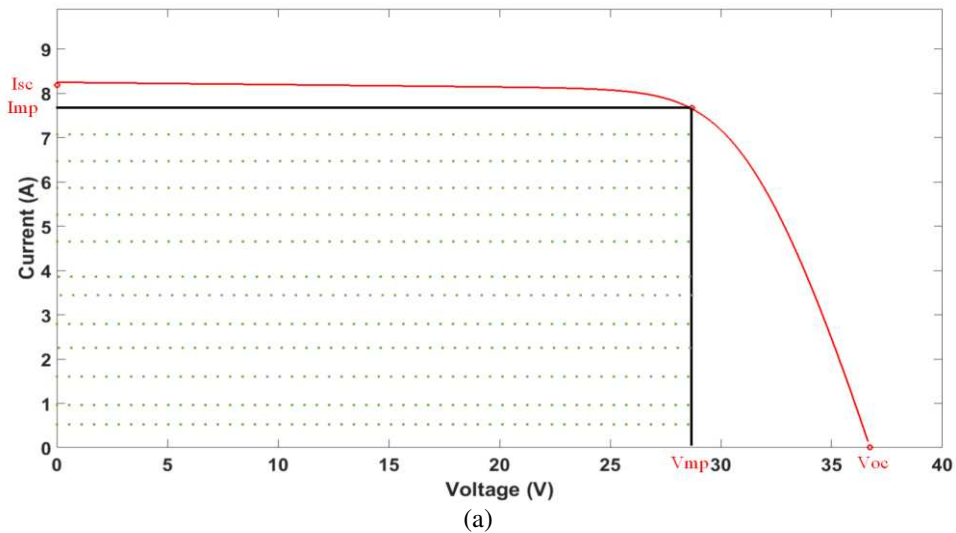


Fig. 5. (a) Fill Factor Parameters Estimation Using Photovoltaic I-V Curve, (b) Fill Factor Estimation under Various Irradiance Levels



### 176 3.3 PV series resistance ( $R_s$ )

#### 177 Method 1:

178 One commonly used method to estimate  $R_s$  is to evaluate the derivative of the voltage with respect to the  
179 current at the  $V_{oc}$ . The final expression to approximate the series resistance is described by (7).

$$180 R_{s,e} = - \left. \frac{dV}{dI} \right|_V \approx V_{oc} = - \left. \frac{V_2 - V_1}{I_2 - I_1} \right|_V \approx V_{oc} \quad (7)$$

181 where  $V_2$ ,  $V_1$ ,  $I_2$  and  $I_1$  are the voltage and the current points estimated near to  $V_{oc}$ .

182 The value of the series resistance estimated by the derivative may vary with the irradiance the temperature  
183 conditions [28]. D. Sara et al [29] proposed a method to translate the value of the estimated  $R_s$  to STC in  
184 order to mitigate the effect of the irradiance ( $G$ ) and PV module temperature ( $T$ ). The expression is  
185 illustrated by (8).

$$186 R_s = R_{s,e} + \frac{V_{te}}{I_{sc}} \left( \frac{G}{G_{STC}} \times \frac{T_{STC}}{T} - 1 \right) \quad (8)$$

187 where  $G_{STC}$  is equal to  $1000 \text{ W/m}^2$  and  $T_{STC}$  is equal to  $25 \text{ }^\circ\text{C}$ .

188 As can be noticed, the estimation of the series resistance requires the voltage and the current measurements  
189 of at least two point of the I-V curve close to the  $V_{oc}$ . The method also requires the value of the irradiance  
190 and the PV modules temperature to perform the estimation of the series resistance value.

#### 191 Method 2:

192 Another method of estimating the series resistance of a PV module is to evaluate the derivative of the  
193 voltage with respect to the current at the short circuit and maximum power point, such point is characterized  
194 by a current lower, but closer to  $I_{mpp}$  and it is denominated as  $Q$ . This method was proposed by [21] and  
195 used in [27 and 28] for the estimation of  $R_s$ . There are two options to calculate  $Q$  (9 & 10).

$$196 Q1 = I_{sc,e} - (0.75 \times I_{mpp}) \quad (9)$$

$$197 Q2 = I_{sc,e} - (0.60 \times I_{mpp}) \quad (10)$$

198 where the value of  $I_{sc,e}$  is the estimated short circuit current and can be evaluated using (11).

$$199 I_{sc,e} = \frac{I_{sc}}{K_1} \quad (11)$$

200 where  $K_1$  is the ratio between  $I_{mpp}$  and  $I_{sc}$  and it is assumed as constant value of 0.92 as described by [21].

201 The final expression of estimating the value of the series resistance is expressed by (12).

$$202 R_s = - \left. \frac{dV}{dI} \right|_I \approx Q = - \left. \frac{V_2 - V_1}{I_2 - I_1} \right|_I \approx Q \quad (12)$$

203 The evaluation of the series resistance requires at least two points of the I-V curve for the PV module.  
204 Furthermore, it is required to measure:

- 205 1. Current at maximum power point ( $I_{mpp}$ )
- 206 2. Short circuit current ( $I_{sc}$ )

207 Fig. 6 shows the value of the series resistance estimated using method 1 and method 2. The estimated values  
 208 of the  $R_s$  are compared with the measured  $R_s$ . Therefore, the difference between the measured values with  
 209 the estimated values can be expressed by (13).

$$210 \quad \text{Difference} = \text{Estimated } R_s - \text{Measured } R_s \quad (13)$$

211 Table 2 shows the comparison between the estimated  $R_s$  and measured  $R_s$  using method 1: at  $V_{oc}$ , and  
 212 method 2: at Q1 and Q2. The minimum average difference is equal to 1.71% obtained for method 1.  
 213 Therefore, in this paper, method 1 is used for the estimation of  $R_s$ .

Table 2  
 Difference between Estimated  $R_s$  and Measured  $R_s$

Irradiance level (W/m <sup>2</sup> )	Measured $R_s$ ( $\Omega$ )	Estimated $R_s$ ( $\Omega$ ) using method 1		Estimated $R_s$ ( $\Omega$ ) using method 2, Q1		Estimated $R_s$ ( $\Omega$ ) using method 2, Q2	
		$R_s$ ( $\Omega$ )	Difference	$R_s$ ( $\Omega$ )	Difference	$R_s$ ( $\Omega$ )	Difference
1000	0.48484	0.512558	0.027717	0.532558	0.047718	0.582558	0.097718
900	0.537836	0.545554	0.007718	0.595554	0.057718	0.595554	0.057718
800	0.567762	0.58548	0.017718	0.62548	0.057718	0.70548	0.137718
700	0.623004	0.637755	0.014751	0.681755	0.058751	0.687755	0.064751
600	0.698996	0.706714	0.007718	0.606714	-0.09228	0.816714	0.117718
500	0.789787	0.804505	0.014718	0.837845	0.048058	0.934505	0.144718
400	0.934482	0.9522	0.017718	0.9822	0.047718	1.1322	0.197718
300	1.172762	1.20048	0.027718	1.23448	0.061718	1.31048	0.137718
200	1.688184	1.705902	0.017718	1.729902	0.041718	1.815902	0.127718
100	3.240672	3.25839	0.017718	3.28139	0.040718	3.33839	0.097718
		Average Difference (%)		Average Difference (%)		Average Difference (%)	
		1.71		3.69		11.81	

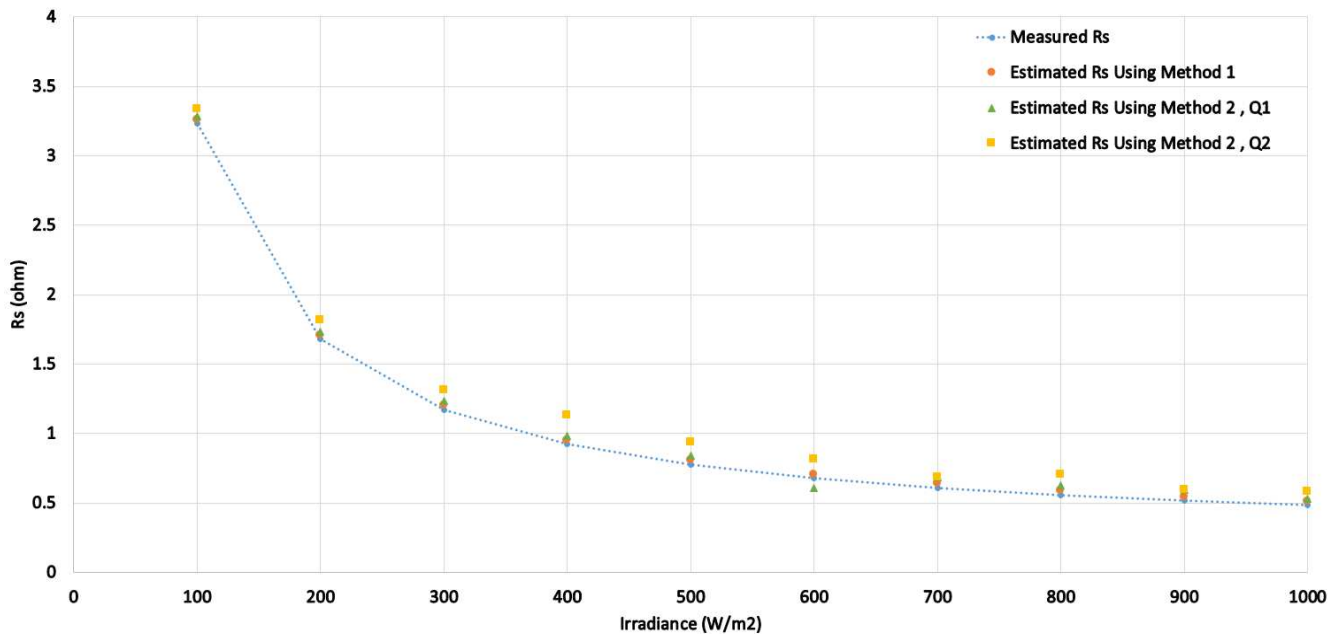


Fig. 6. Evaluating the Series Resistance of a PV Module under Various Irradiance Levels

214 **4. Simulation, modelling and data analysis of multiple PV array configurations**

215 The aim of this section is to present the multiple PV array configurations used in this study. In order to test  
 216 the multiple PV array configurations, 24 PV modules were used. Each PV module consists of 60 PV  
 217 modules connected in series and protected by bypass diodes. The PV modules temperature was fixed at the  
 218 standard test condition (STC) 25 °C.

219 **4.1 Types of examined PV array configurations**

220 Five common PV array configurations were used in order to examine the main indicators which are mostly  
 221 changeable during the normal operation mode, partial shading and faulty PV conditions. The examined PV  
 222 array configurations are listed as the following:

- 223 1. Series (S) configuration
- 224 2. Parallel (P) configuration
- 225 3. Series-Parallel (SP) configuration
- 226 4. Total-Cross-Tied (TCT) configuration
- 227 5. Bridge-Linked (BL) configuration

228 MATLAB/Simulink software is used to create the listed PV array configurations. Appendix A contains all  
 229 MATLAB/Simulink software models which are used to configure the grid-connected PV (GCPV) systems.  
 230 Furthermore, during the simulation all indicators:  $V_{mpp}$ ,  $V_{oc}$ ,  $I_{mpp}$ ,  $I_{sc}$ ,  $P_{mpp}$ ,  $R_s$ , FF and  $V_{te}$  were saved in a  
 231 spreadsheet to evaluate the performance of each PV array configuration separately.

232 **4.2 PV array configurations under STC**

233 This section presents the variations of all required indicators at standard test conditions applied to the PV  
 234 array configurations. Table 3 shows the value of all indicators for the different PV array configurations.  
 235 The main outcomes from the obtained results can be expressed by the following:

- 236 1. Series configuration: the dominant indicator is the value of the  $V_{oc}$ ,  $V_{mp}$  and the value of the thermal  
 237 voltage.
- 238 2. Parallel configuration:  $I_{sc}$ ,  $I_{mpp}$  and the thermal voltage which has the least value across all PV  
 239 configurations.
- 240 3. SP, TCT and BL configurations have a common similarity across all indicators.
- 241 4. At STC, the FF for all PV configurations is approximately equal to 73.2%.

242 From Table 4 it is possible to evaluate the value of the series resistance across one PV module in the GCPV  
 243 systems according to the mathematical expressions listed below in Table 3.

Table 3  
 Mathematical Calculations of  $R_s$  for Various GCPV Plants

PV array configuration	Mathematical expression for estimating the value of $R_s$ for one PV module in the PV array configuration	
S	$\frac{R_s \text{ (Obtained from the I-V Curve)}}{24_{\text{(total PV module in the PV array configuration)}}$	(14)
P	$R_s \text{ (Obtained from the I-V Curve)} \times 24_{\text{(total PV module in the PV array configuration)}}$	(15)
SP, TCT and BL	$\frac{R_s \text{ (Obtained from the I-V Curve)} \times 4_{\text{(number of PV columns)}}}{6_{\text{(number of PV modules in one PV row "PV String")}}}$	(16)

244 Table 5 shows that the estimation of the series resistance for a single PV module using the mathematical  
 245 expressions listed in Table 3 at STC. There is a slightly difference between the real measured  $R_s$  values at  
 246 STC with the calculated  $R_s$  using (14-16). The percentage of the average difference between the measured  
 247  $R_s$  and the calculated  $R_s$  is equal to 2.2%.

Table 4  
 Indicators Values Estimated for All Examined PV Array Configurations

PV configuration	$I_{sc}$ (A)	$V_{oc}$ (V)	$I_{mpp}$ (A)	$V_{mpp}$ (V)	$P_{mpp}$ (W)	$R_s$ ( $\Omega$ )	$V_{te}$ (V)	FF (%)
S	8.177	881.2	7.538	700.3	5279	12.18175	36.2059	73.2608
P	196.2	36.74	181.4	29.1	5279	0.020116	1.44597	73.2305
SP	32.71	220.3	30.26	174.4	5279	0.757576	8.59957	73.2353
TCT	32.71	220.3	30.33	174	5278	0.757576	8.31149	73.2363
BL	32.71	220.3	30.33	174	5278	0.757576	8.31149	73.2363

Table 5  
 Estimated  $R_s$  for One PV Module Only

PV configuration	$R_s$ ( $\Omega$ )	Calculated $R_s$ for one PV module ( $\Omega$ )	Measured $R_s$ for one PV module at STC ( $\Omega$ )	Difference in the estimation of $R_s$ (%)
S	12.18175	0.507573	0.48484	2.273299
P	0.020116	0.482772	0.48484	-0.20675
SP	0.757576	0.505051	0.48484	2.021051
TCT	0.757576	0.505051	0.48484	2.021051
BL	0.757576	0.505051	0.48484	2.021051

### 248 4.3 Partial shading conditions applied to the PV array configurations

249 In order to evaluate the behavior of each PV configuration under non-uniform irradiance conditions and to  
 250 choose the most optimal configuration that provides that highest performance and identifying the main  
 251 indicators which are changing significantly in each PV configuration, two different shading scenarios and  
 252 two faulty PV conditions were tested for each PV configuration under a fixed temperature 25 °C.

#### 253 4.3.1 Scenario 1: row level

254 In this part, the focus will be on the performance of the PV configurations which are affected by a uniformly  
 255 and non-uniform shading patterns on a row level (row of PV modules). Fig. 7 shows both patterns used to  
 256 evaluate the row shading conditions effects on the PV modules.

257 As can be noticed from Fig. 7, two different partial shading conditions was performed. The first partial  
 258 shading pattern is applied on a row of PV modules at irradiance level equal to 500 W/m<sup>2</sup>. However, the  
 259 second shading pattern consists of various irradiance levels (200, 400, 600 and 800 W/m<sup>2</sup>) applied to four  
 260 PV modules.

261 Fig. 8(a) shows the maximum output power obtained in each PV array configuration under shading pattern  
 262 1. The P configuration shows the maximum output power comparing to all other examined PV array  
 263 configurations. The configurations S, SP, TCT and BL provide the same maximum power in each case.

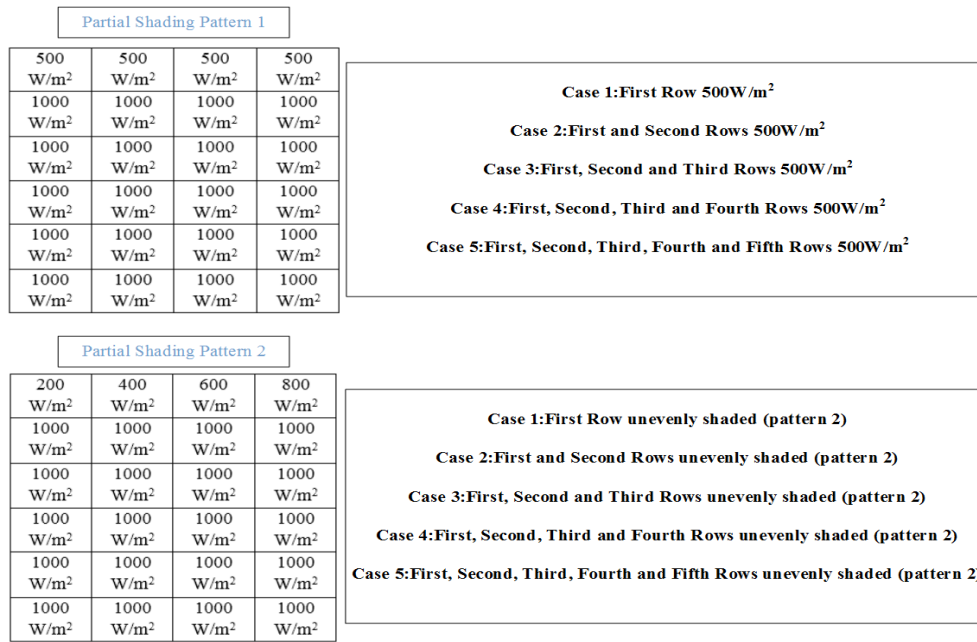


Fig. 7. Partial Shading Patterns for Scenario 1: Row Level

264 Fig. 8(b) proves that P configuration has the maximum output power among all other PV array  
 265 configurations under shading pattern 2. TCT and BL comes second best choice whereas the series  
 266 configuration has the lowest performance.

267 In each shading pattern, the series resistance ( $R_s$ ) was estimated using method 1 which has been discussed  
 268 previously in section 3.3. Table 6 shows the estimated  $R_s$  for each PV array configuration for shading  
 269 pattern 1.  $R_s$  estimated for the S configuration is increased by approximate to 1.13  $\Omega$ . Additionally, the  
 270 estimated series resistance for SP, TCT and BL configurations is increased by approximate to 0.07  $\Omega$ . There  
 271 is a very small amount of change in the series resistance obtained for P configuration, the reduction is only  
 272 equal to 0.002  $\Omega$ .

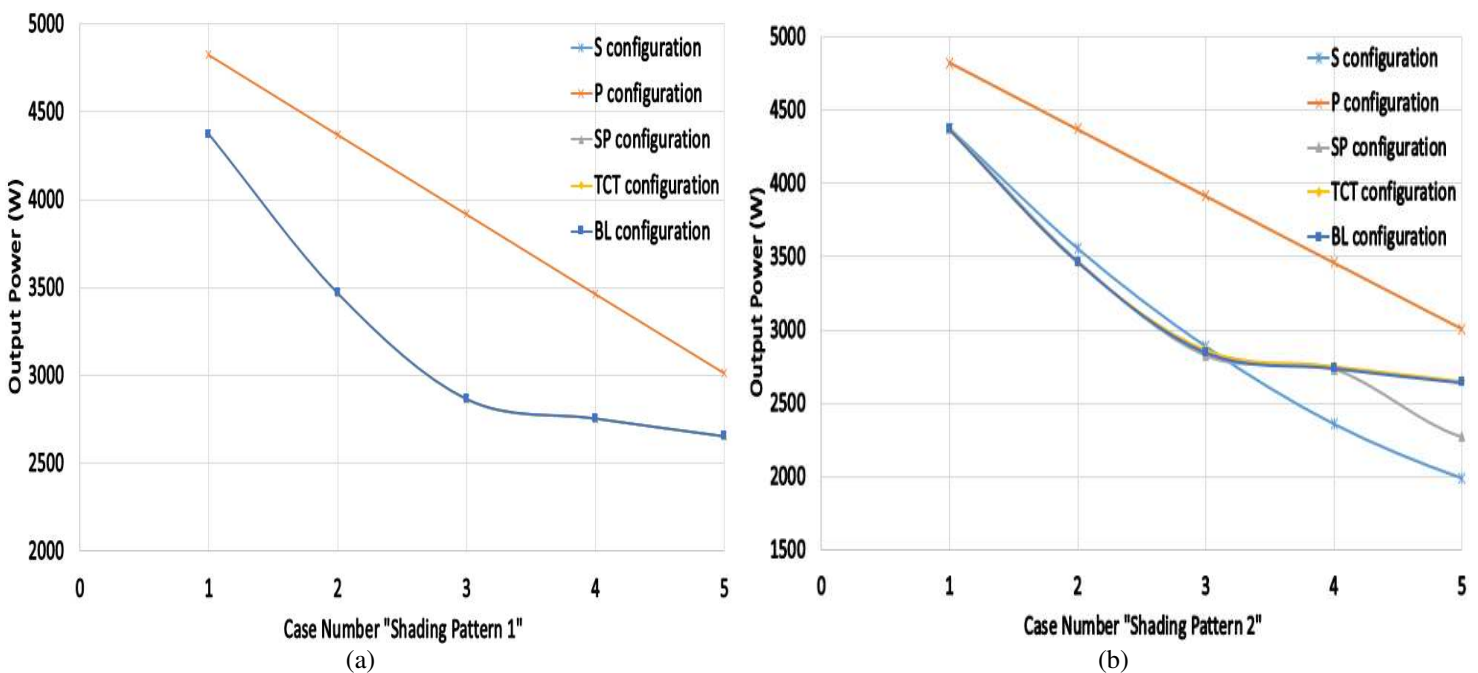


Fig. 8. Partial Shading Patterns for Scenario 1: Row Level. (a) Output Power for Pattern 1, (b) Output power for Pattern 2

Table 6  
Estimated  $R_s$  for the Multiple Array Configurations, Scenario 1: Row Level, Pattern 1

Case #	Estimated $R_s$ ( $\Omega$ ) for Shading Pattern 1				
	S	P	SP	TCT	BL
Case 1	13.33689	0.022147	0.826446	0.826446	0.826446
Case 2	14.47387	0.023601	0.897666	0.897666	0.897666
Case 3	15.61524	0.025198	0.966184	0.966184	0.966184
Case 4	16.7392	0.027174	1.037344	1.037344	1.037344
Case 5	17.87949	0.029661	1.105705	1.105705	1.105705

Table 7  
Estimated  $R_s$  for the Multiple Array Configurations, Scenario 1: Row Level, Pattern 2

Case #	Estimated $R_s$ ( $\Omega$ ) for Shading Pattern 2				
	S	P	SP	TCT	BL
Case 1	14.05877	0.022279	0.848896	0.827267	0.835422
Case 2	15.9261	0.023609	0.921404	0.898473	0.906618
Case 3	17.75884	0.025253	0.990099	0.968992	0.975039
Case 4	19.604	0.027216	1.053297	1.037775	1.045369
Case 5	21.42704	0.029775	1.136493	1.109385	1.117318

273 Table 7 shows the estimated  $R_s$  for partial shading pattern 2. The S configuration has an increase by 1.8  $\Omega$   
 274 in the  $R_s$ . Moreover, the parallel configuration has the lowest rate of change in the  $R_s$  which is approximate  
 275 equal to 0.002. SP, TCT and BL configurations has an increase of 0.07  $\Omega$  in the  $R_s$  among all testes cases  
 276 in the row level partial shading conditions.

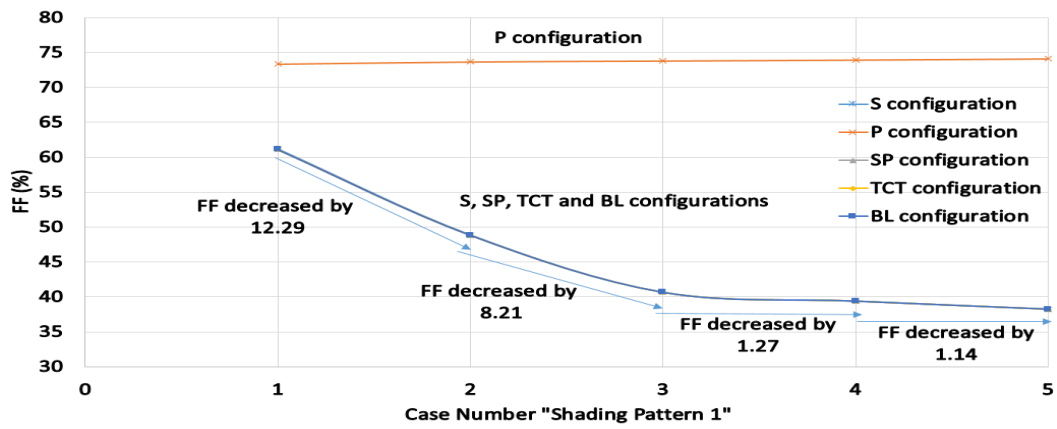
277 The FF indicator was also calculated for each examined partial shading patterns. Fig. 9(a) and Fig 9(b)  
 278 illustrates the FF variations among the tested GCPV systems for shading pattern 1 and shading pattern 2  
 279 respectively. The P configuration shows that the FF has a value close to 73% among all tested case  
 280 scenarios. However, a reduction in the FF was obtained across all other PV array configurations.

281 The Thermal voltage  $V_{te}$  across each PV array configuration during the tested partial shading pattern1 and  
 282 pattern 2 are shown in Fig. 9(c) and Fig. 9(d) respectively. The threshold values of the  $V_{te}$  is taken from  
 283 Table 4. It is evident that the  $V_{te}$  for P configuration is approximate equal to 1.44V which is exactly the  
 284 same as the P configuration  $V_{te}$  threshold.

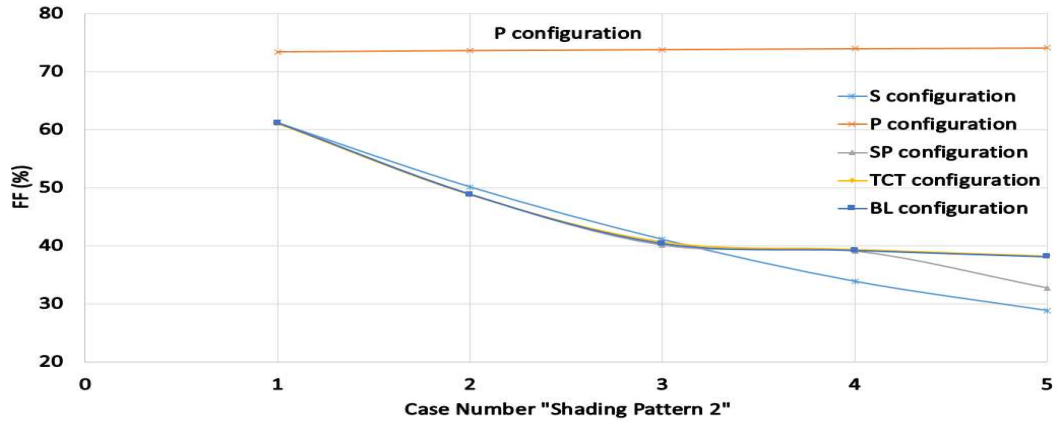
285 S, SP, TCT and BL configurations show that the value of  $V_{te}$  is lower than the value of  $V_{te}$  threshold in low  
 286 partial shading conditions if: reduction in irradiance < 6000 W/m<sup>2</sup>. However, in most partial shading  
 287 conditions examined in this section, the obtained value of the  $V_{te}$  is greater than the value of  $V_{te}$  threshold  
 288 if: reduction in the irradiance  $\geq$  6000 W/m<sup>2</sup>.

289 From this section, the obtained results could be illustrated as the following:

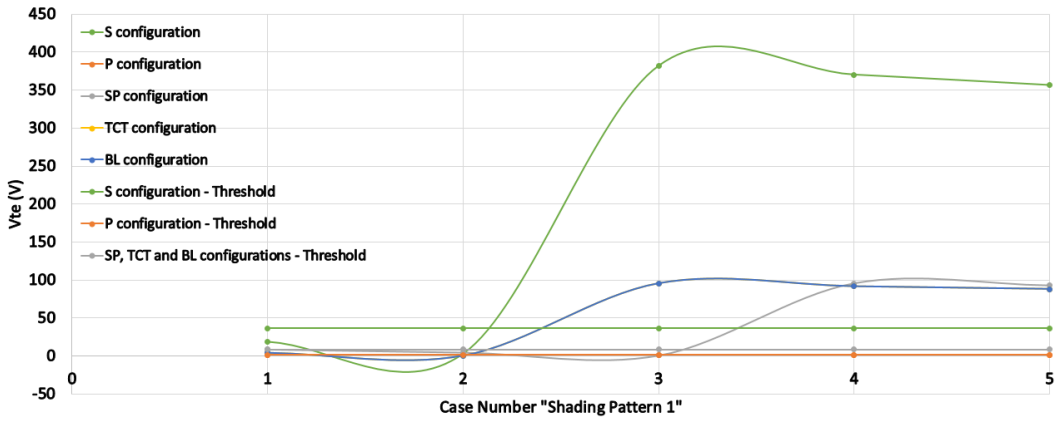
- 290 •  $R_s$  could be a good indicator to predict/estimate partial shading conditions for S, SP, TCT and BL  
 291 configurations. However,  $R_s$  cannot be used with P configuration since it does not change  
 292 significantly during the increase/decrease of the partial shading conditions applied PV system.
- 293 • FF has a significant drop in its value while increasing the partial shading in the S, SP, TCT and BL  
 294 configurations. This is not a proper indicator to be used with P configuration since it does not  
 295 change among all tested partial shading conditions.
- 296 • When the reduction in the irradiance is greater or equal to 6000 W/m<sup>2</sup>, the value of the  $V_{te}$  in most  
 297 partial shading conditions is greater than the value of  $V_{te}$  threshold for S, SP, TCT and BL  
 298 configurations. However, P configurations shows that the value of the  $V_{te}$  is almost equal to the  
 299 value of  $V_{te}$  threshold.



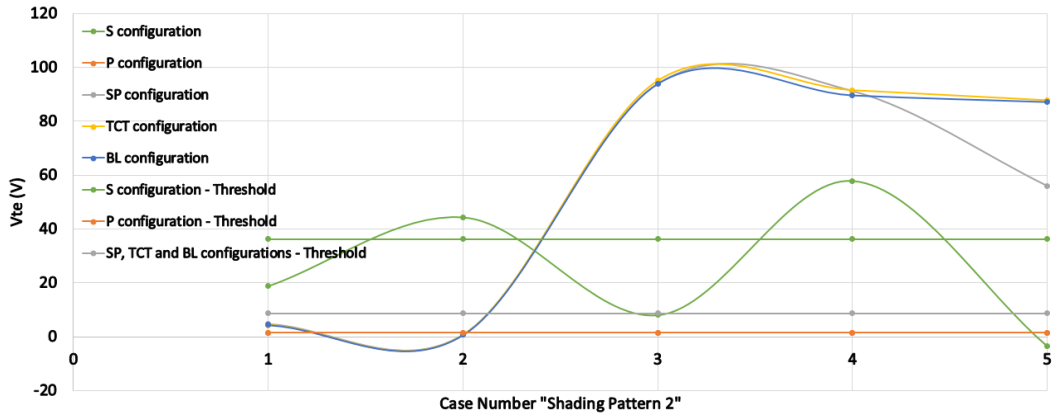
(a)



(b)



(c)



(d)

Fig. 9. FF and  $V_{te}$  Variations for Scenario 1: Row Level. (a) Fill Factor Variations for Pattern 1, (b) Fill Factor Variations for Pattern 2, (c)  $V_{te}$  Variations for Pattern 1, (d)  $V_{te}$  Variations for Pattern 2

300 **4.3.2 Scenario 2: column level**

301 This section is created to check the variations of the  $R_s$ ,  $V_{te}$ , FF indicators when a partial shading conditions  
 302 occurred in the PV array configuration on a column level (column of PV modules).

303 Fig. 10 shows two different partial shading patterns examined. The first partial shading pattern is applied  
 304 on a column of PV modules at irradiance level equal to 500 W/m<sup>2</sup>. However, the second shading pattern  
 305 consists of various irradiance levels (100, 200, 500, 600, 800 and 900 W/m<sup>2</sup>) applied to six PV modules.

306 Fig. 11(a) shows the maximum output power obtained in each PV array configuration under shading pattern  
 307 1. P, SP, TCT and BL configurations shows approximately the same maximum output power. Furthermore,  
 308 S configuration provides the minimum output power during all examined case scenarios used in shading  
 309 pattern 1. On the other hand, the maximum output power obtained from shading pattern 2 is illustrated in  
 310 Fig. 11(b). The maximum output power could be evaluated at the P configuration. However, S configuration  
 311 remains the worst configuration.

312 In each shading pattern (pattern 1 and 2), the series resistance ( $R_s$ ) was estimated. Table 8 shows the  
 313 estimated  $R_s$  for each PV array configuration for shading pattern 1. As can be noticed,  $R_s$  estimated for the  
 314 S configuration is increasing by approximate to 1.68  $\Omega$ . This result can be calculated using the difference  
 315 between case1 and case2, where the values of  $R_s$  are taken from the measured data explained in table 2:

316  $Estimated R_s = \text{Number of PV modules (at partial shading condition)} \times R_s \text{ (at partial shading condition)}$

317  $Case1: Estimated R_s = \left( 6_{(at 500 \frac{W}{m^2})} \times 0.789787 \right) + \left( 18_{(at 1000 \frac{W}{m^2})} \times 0.48484 \right) = 13.47 \Omega$

318  $Case2: Estimated R_s = \left( 12_{(at 500 \frac{W}{m^2})} \times 0.789787 \right) + \left( 12_{(at 1000 \frac{W}{m^2})} \times 0.48484 \right) = 15.30 \Omega$

319  $Difference = Case2 - Case1 = 15.3 - 13.47 = 1.83 \Omega \approx 1.68 \Omega$  Obtained by the I – V cuve

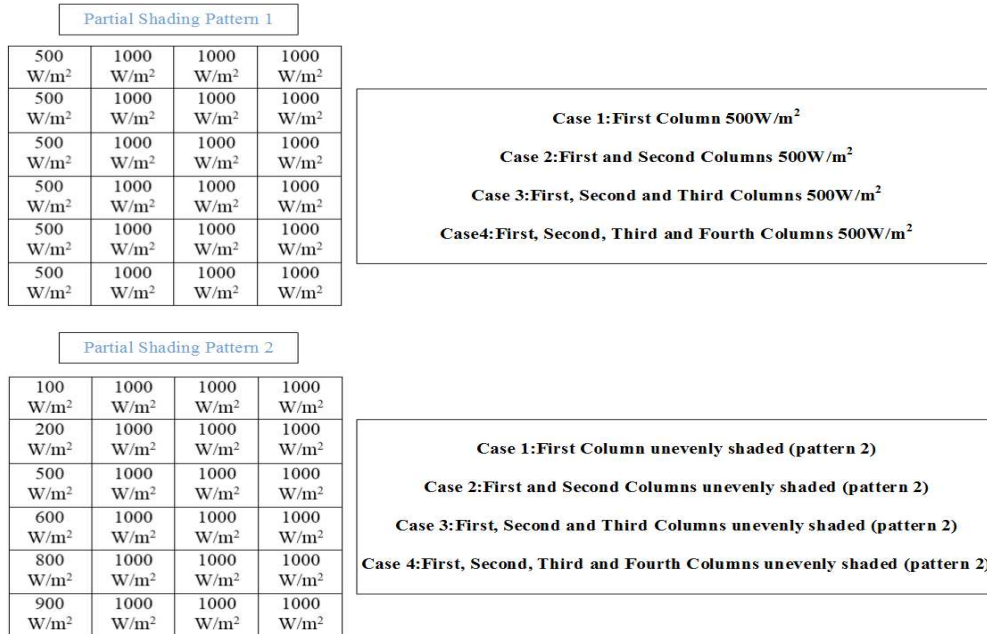


Fig. 10. Partial Shading Patterns for Scenario 2: Column Level



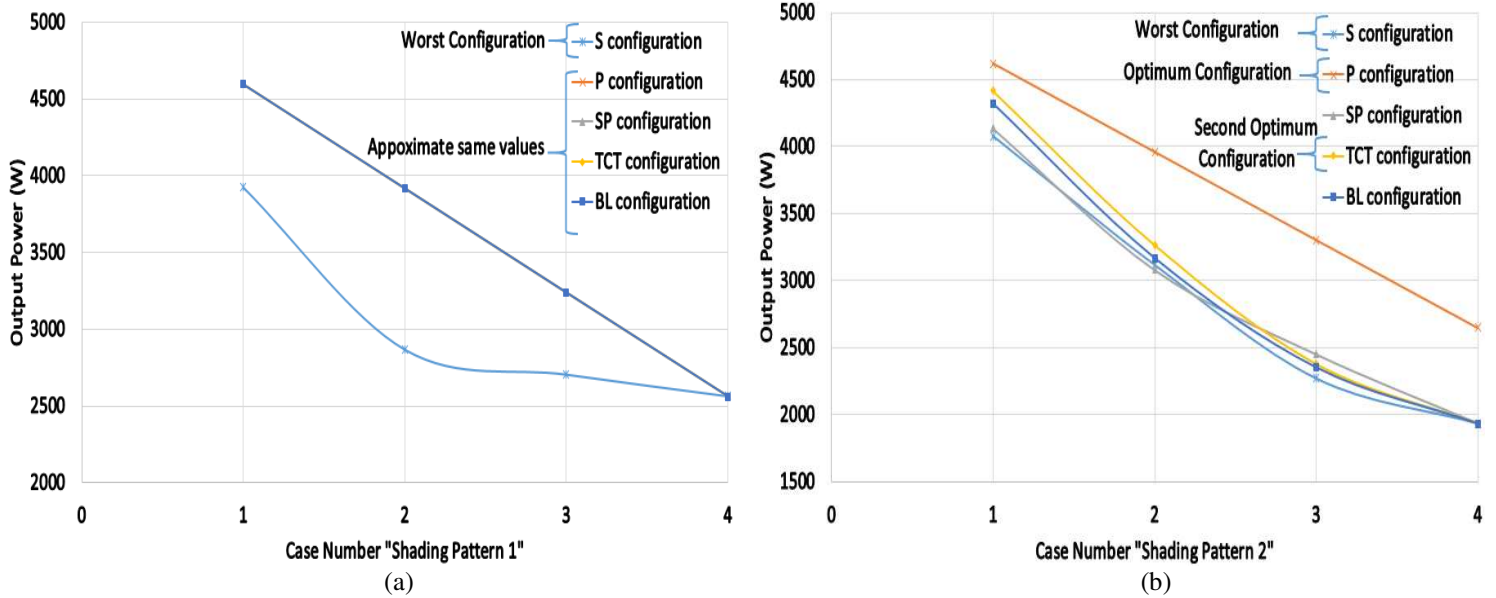


Fig. 11. Partial Shading Patterns for Scenario 2: Column Level. (a) Output Power for Pattern 1, (b) Output power for Pattern 2

320 Additionally, the estimated series resistance for SP, TCT and BL configurations is increasing by  
 321 approximate to  $0.12 \Omega$ . However, the parallel configuration remains at nearly constant series resistance  
 322 between  $0.02 - 0.03 \Omega$ .

323 For the second shading pattern (non-uniform irradiance) the estimated  $R_s$  for SP, TCT and BL  
 324 configurations is increasing by  $0.3 \Omega$ . The parallel configuration remains at the same  $R_s$  which is between  
 325  $0.02 - 0.03 \Omega$ . Similarly, the estimated series resistance for S configuration is increasing by  $4.4 \Omega$  while  
 326 increasing the applied partial shading on the PV array configuration, this can be seen in Table 9 and  
 327 described by the following mathematical calculations, where the values of  $R_s$  are taken from the measured  
 328 data explained in table 2:

329  $Measured R_s = \text{Number of PV modules (at partial shading condition)} \times R_s \text{ (at partial shading condition)}$

330 *Case1: Measured  $R_s$*

331 
$$= \left( 1_{\left( \text{at } 100 \frac{W}{m^2} \right)} \times 3.241 \right) + \left( 1_{\left( \text{at } 200 \frac{W}{m^2} \right)} \times 1.688 \right) + \left( 1_{\left( \text{at } 500 \frac{W}{m^2} \right)} \times 0.789787 \right)$$
  
 332 
$$+ \left( 1_{\left( \text{at } 600 \frac{W}{m^2} \right)} \times 0.6988 \right) + \left( 1_{\left( \text{at } 800 \frac{W}{m^2} \right)} \times 0.5677 \right) + \left( 1_{\left( \text{at } 900 \frac{W}{m^2} \right)} \times 0.5378 \right)$$
  
 333 
$$+ \left( 18_{\left( \text{at } 1000 \frac{W}{m^2} \right)} \times 0.48484 \right) = 16.25 \Omega$$

334 *Case2: Measured  $R_s$*

335 
$$= \left( 2_{\left( \text{at } 100 \frac{W}{m^2} \right)} \times 3.241 \right) + \left( 2_{\left( \text{at } 200 \frac{W}{m^2} \right)} \times 1.688 \right) + \left( 2_{\left( \text{at } 500 \frac{W}{m^2} \right)} \times 0.789787 \right)$$
  
 336 
$$+ \left( 2_{\left( \text{at } 600 \frac{W}{m^2} \right)} \times 0.6988 \right) + \left( 2_{\left( \text{at } 800 \frac{W}{m^2} \right)} \times 0.5677 \right) + \left( 2_{\left( \text{at } 900 \frac{W}{m^2} \right)} \times 0.5378 \right)$$
  
 337 
$$+ \left( 12_{\left( \text{at } 1000 \frac{W}{m^2} \right)} \times 0.48484 \right) = 20.865 \Omega$$

338  $Difference = Case2 - Case1 = 20.865 - 16.25 = 4.6 \Omega \approx 4.4 \Omega$  Obtained by the I - V cuve

Table 8

Estimated $R_s$ for the Multiple Array Configurations, Scenario 2: Column Level, Pattern 1					
Case #	Estimated $R_s$ ( $\Omega$ ) for Shading Pattern 1				
	S	P	SP	TCT	BL
Case 1	13.8754	0.022921	0.818197	0.818197	0.818197
Case 2	15.55936	0.025198	0.898957	0.898957	0.898957
Case 3	17.26519	0.028329	1.012146	1.012146	1.012146
Case 4	18.93581	0.033034	1.176471	1.176471	1.176471

Table 9  
Estimated  $R_s$  for the Multiple Array Configurations, Scenario 2: Column Level, Pattern 2

Case #	Estimated $R_s$ ( $\Omega$ ) for Shading Pattern 2				
	S	P	SP	TCT	BL
Case 1	16.85772	0.022861	0.83675	0.819403	0.823045
Case 2	21.33106	0.025054	0.961538	0.918274	0.929195
Case 3	25.75992	0.02809	1.186662	1.106195	1.119821
Case 4	30.08424	0.032468	1.845018	1.845359	1.845359

339 Fig. 12(a) and Fig. 12(b) illustrates the FF variations among the tested PV array configuration systems for  
 340 shading pattern 1 and shading pattern 2 respectively. Shading pattern 1 shows that P, SP, TCT and BL  
 341 configurations have a value of FF approximate to 74% among all tested cases. However, a reduction in the  
 342 FF was only obtained across the S configuration. Shading pattern 2 (non-uniform shading) shows a different  
 343 results comparing to shading pattern 1 (uniform shading), these results could be illustrated as the following:

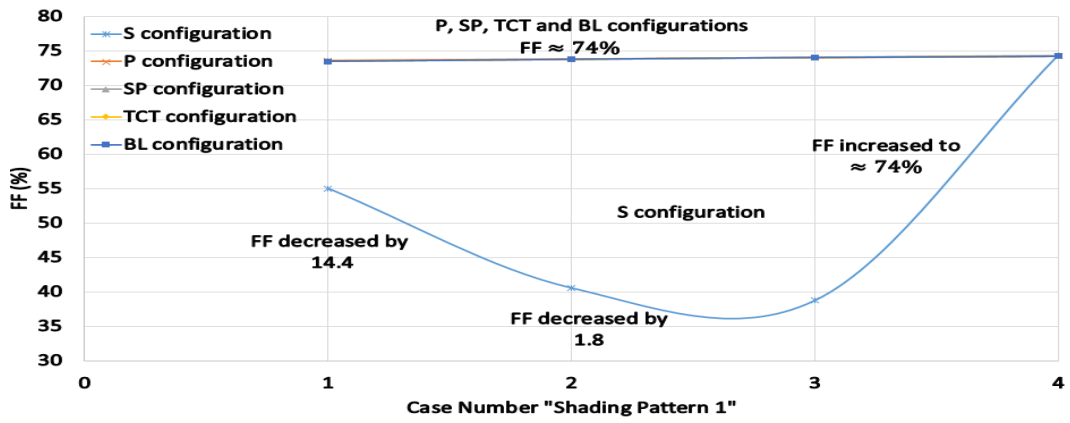
- 344 • The estimated FF for the P configuration under non-uniform and uniform shading patterns are  
 345 exactly equal.
- 346 • There is a huge reduction in the FF for S, SP, TCT and BL configurations in the non-uniform  
 347 shading pattern conditions.
- 348 • Fig. 12(a) shows that the value of the FF for the S configuration at case 4 is equal to 74% because  
 349 in this particular shading case, the percentage of shading among all PV modules are equal.

350 The Thermal voltage  $V_{te}$  across each PV array configuration during the tested partial shading pattern1 and  
 351 pattern 2 are shown in Fig. 12(c) and Fig. 9(d) respectively. The threshold values of the  $V_{te}$  is taken from  
 352 Table 4. It is evident that the  $V_{te}$  for P configuration is approximate equal to 1.44V which is exactly the  
 353 same as the P configuration  $V_{te}$  threshold. The estimated values of the  $V_{te}$  for SP, TCT and BL  
 354 configurations are exactly the same as the  $V_{te}$  threshold during shading pattern 1. However, the estimated  
 355  $V_{te}$  for S configuration is greater than the value of the  $V_{te}$  threshold if: Reduction in irradiance  $\geq 6000$  W/m<sup>2</sup>.

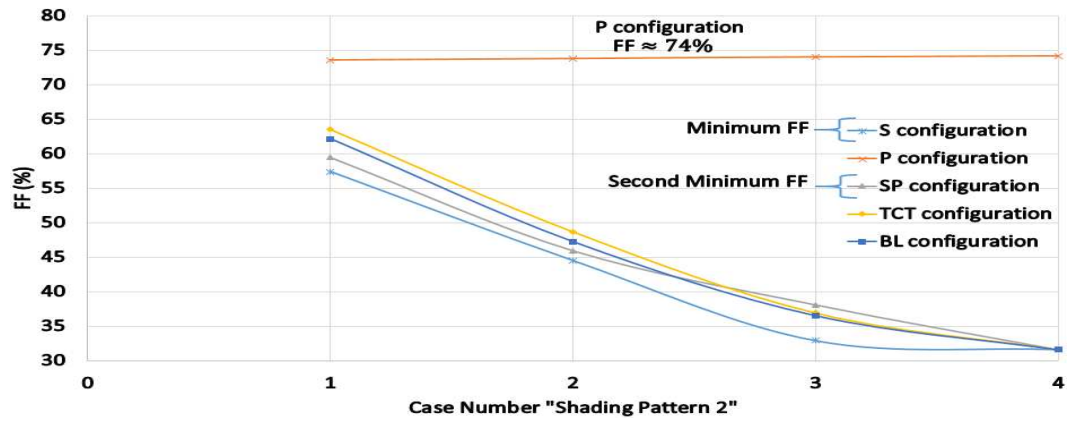
356 Fig. 12(d) shows that the estimated  $V_{te}$  is exactly the same as the  $V_{te}$  threshold for shading pattern 2. SP,  
 357 TCT and BL configurations proves that when the reduction in the irradiance is greater than 2900 W/m<sup>2</sup>  
 358 the estimated value of  $V_{te}$  is always greater than  $V_{te}$  threshold. Moreover, S configuration shows that the  
 359 value of the  $V_{te}$  is greater than  $V_{te}$  threshold if: Reduction in irradiance  $\geq 6000$  W/m<sup>2</sup>.

360 In conclusion, this section shows some results on the performance of the examined PV array configurations  
 361 under uniform and non-uniform partial shading patterns. The main findings could be illustrated as the  
 362 following:

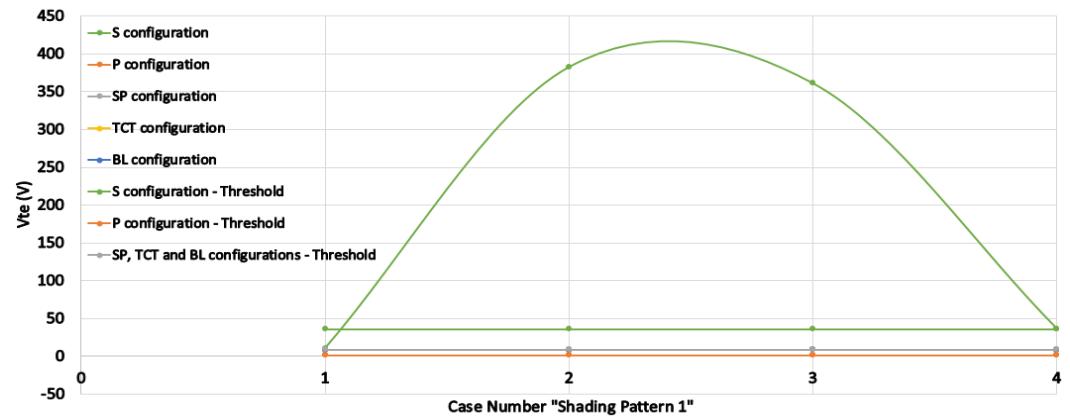
- 363 • Under uniform shading patterns which effects on a column of PV modules, the output power for P,  
 364 SP, TCT and BL configurations are exactly the same. Furthermore, the S configuration shows the  
 365 least output power among all PV array configurations.
- 366 • Under non-uniform shading patterns which effects on a column of PV modules, the optimum output  
 367 power was estimated for the parallel configuration.
- 368 • The series resistance  $R_s$  is a good indicator for detecting/predicting partial shading conditions for  
 369 S, SP, TCT and BL configurations since the value of the  $R_s$  change significantly while increasing  
 370 the partial shading conditions applied to the PV configurations.
- 371 • The Fill factor (FF) indicator could be used with SP, TCT and BL configurations only under non-  
 372 uniform irradiance conditions. Furthermore, there is a large drop in the value of FF for the S  
 373 configuration under uniform and non-uniform irradiance levels.
- 374 • The value of the  $V_{te}$  could be used as a proper indicator for detecting partial shading conditions for  
 375 S, SP, TCT and BL configuration under non-uniform partial shading conditions affecting the GCPV  
 376 plants.



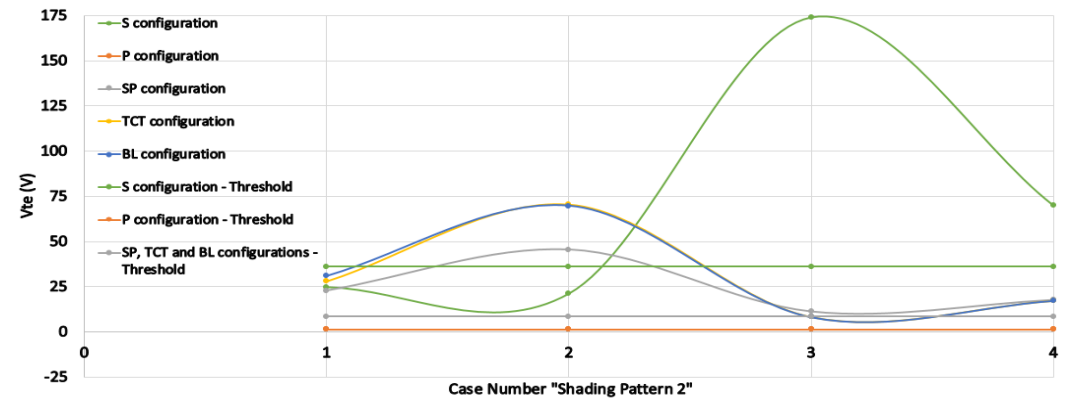
(a)



(b)



(c)



(d)

Fig. 12. FF and  $V_{te}$  Variations for Scenario 2: Column Level. (a) Fill Factor Variations for Pattern 1, (b) Fill Factor Variations for Pattern 2, (c)  $V_{te}$  Variations for Pattern 1, (d)  $V_{te}$  Variations for Pattern 2

### 377 4.3.3 Scenario 3: faulty PV modules

378 This section is created to check the variations of the  $R_s$ ,  $V_{te}$ , FF indicators when a faulty PV modules have  
379 been a raised in the PV array configurations.

380 Two faulty scenarios were carried out to estimate the output performance for each PV array configuration  
381 under faulty PV modules. Fig. 13 illustrates both cases which can be described by the following:

- 382 1. Row level: six different scenarios were tested to estimate the faulty PV modules which are  
383 disconnected (short circuit the PV module) from a row of the PV array configuration.
- 384 2. Column level: four different scenarios were tested to estimate the faulty PV modules which are  
385 disconnected from the entire column of the PV array configuration.

386 The PV modules irradiance and temperature level are at standard test conditions:  $1000W/m^2$  and  $25\text{ }^\circ C$   
387 respectively.

388 Fig. 14(a) and Fig 14(b) shows that the configurations S and P provides the highest maximum output power  
389 among all PV array configurations. The second maximum output power is achieved by the SP configuration.  
390 However, the minimum output power is estimated for the TCT configuration among all faulty PV case  
391 scenarios.

392 The estimated series resistance  $R_s$  for the row-level PV faulty conditions are illustrated in Table 10. The S  
393 configuration shows that  $R_s$  is decreasing by  $0.49\ \Omega$  while disconnecting one PV module. This result is  
394 approximate equal to the measured value of  $R_s$  among one PV module ( $0.48484\ \Omega$ ) under STC as shown  
395 previously in Table 5.

396 The estimated  $R_s$  for the P configuration among all faulty scenarios is approximately equal to  $0.02\ \Omega$ . The  
397 value of  $R_s$  when a PV string is disconnected from the PV array configuration is equal to  $1.007\ \Omega$  for SP,  
398 TCT and BL configurations, this value cloud be calculated using (16) as the following:

$$399 \quad \text{Estimated } R_s \text{ for one PV module} = \frac{R_s \text{ (Obtained from the I-V Curve)} \times 3 \text{ (number of PV columns)}}{6 \text{ (number of PV modules in one PV row "PV String")}}$$
$$400 \quad 0.48484 = \frac{R_s \text{ (Obtained from the I-V Curve)} \times 3 \text{ (Since one PV string is completely disconnected)}}{6}$$

$$401 \quad R_s \text{ (Obtained from the I-V Curve)} = 0.97\ \Omega \approx 1.007\ \Omega$$

402 The estimated series resistance  $R_s$  for the column-level PV faulty conditions are illustrated in Table 11. As  
403 can be noticed that the value of  $R_s$  in the S and SP configurations is decreased while increasing the number  
404 of faulty PV modules. The estimated  $R_s$  for TCT and BL is increasing for the first three PV faulty conditions.  
405 However, the estimated  $R_s$  is equal to  $0.63\ \Omega$  when disconnecting an entire PV column form the SP, TCT  
406 and BL array configurations. This result could be estimated using (16) as the following:

$$407 \quad \text{Estimated } R_s \text{ for one PV module} = \frac{R_s \text{ (Obtained from the I-V Curve)} \times 4 \text{ (number of PV columns)}}{5 \text{ (number of PV modules in one PV row "PV String")}}$$
$$408 \quad 0.48484 = \frac{R_s \text{ (Obtained from the I-V Curve)} \times 4 \text{ (Since one PV string is completely disconnected)}}{5}$$

$$409 \quad R_s \text{ (Obtained from the I-V Curve)} = 0.61\ \Omega \approx 0.63\ \Omega$$

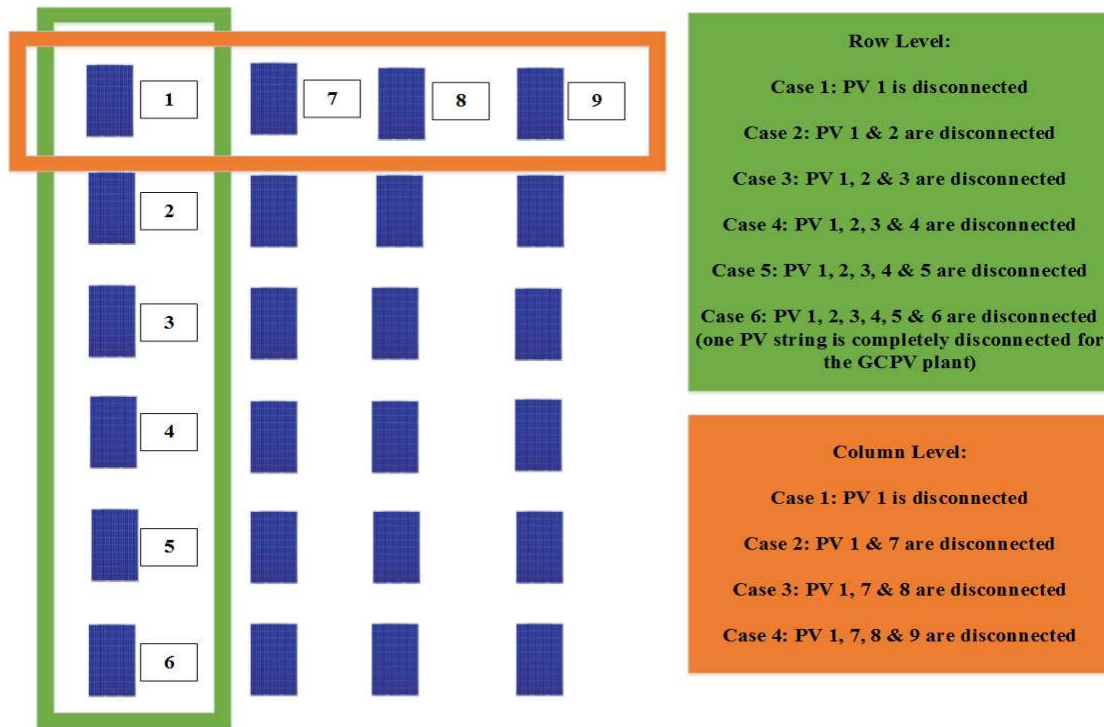


Fig. 13. PV Faulty Conditions for Scenario 3: Faulty PV Modules

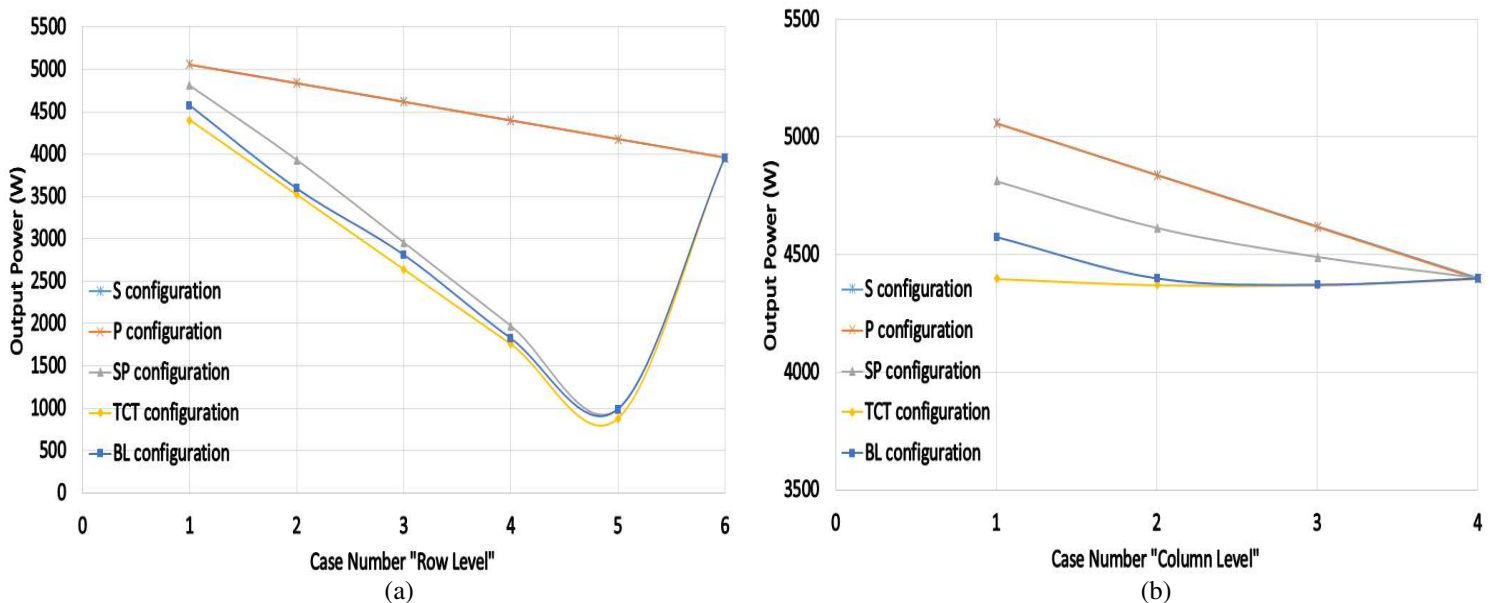


Fig. 14. Output Power for Scenario 3: Faulty PV Modules. (a) Output Power for Pattern 1, (b) Output power for Pattern 2

410 Fig. 15(a) and Fig. 15(b) illustrates the FF variations among the tested PV array configurations using faulty  
 411 conditions: row-level and column level respectively. Row-level PV faulty conditions show that S, P and  
 412 TCT configurations have a value of FF approximate to 73.2% among all tested scenarios. However, a  
 413 reduction in the FF was only obtained across the SP and BL configurations.

414 The column-level PV faulty conditions shows that the FF for the S and P configuration remains at 73.2%.  
 415 Furthermore, there is a huge reduction in the estimated FF for both TCT and BL configurations. The only  
 416 configuration which has an increase in the estimated values of the FF was obtained for the SP configuration.

417 As shown in Fig. 15(a) at case 6 (Faulty PV string) the estimated value of the FF across all PV array  
 418 configurations is equal to 73.2%. Similar results obtained for case4 (faulty column) illustrated in Fig 15(b).

419 The Thermal voltage  $V_{te}$  estimated for each PV array configuration under faulty PV modules conditions  
 420 (row-level and column-level) are shown in Fig. 15(c) and Fig. 9(d) respectively. From Fig. 15(c), it is  
 421 evident that  $V_{te}$  for P configuration is equal to 1.36V among all PV faulty conditions, this result is  
 422 approximately equal to P configuration  $V_{te}$  threshold: 1.44V. The estimated value of the  $V_{te}$  for S, SP, TCT  
 423 and BL configurations is decreased while increasing the number of faulty PV modules in the PV array  
 424 configuration due to the decrease in the  $V_{mp}$ . Despite the decrease of  $V_{oc}$ , the value of  $V_{mp}$  is multiplied by  
 425 a factor of 2, therefore,  $V_{te}$  is also decreasing. This results can be expressed by the following:

426 
$$V_{te} \downarrow = \frac{(2V_{mp} \downarrow - V_{oc} \downarrow)(I_{sc} - I_{mp})}{I_{mp} - (I_{sc} - I_{mp}) \ln\left(\frac{I_{sc} - I_{mp}}{I_{sc}}\right)}$$

427 Different results obtained at case6 in Fig. 15(c), where a faulty PV string occurred in each PV configuration.  
 428 The value of  $V_{te}$  for the SP, TCT and BL is increased because the value of the  $I_{sc}$  and  $I_{mp}$  is decreased:

429 
$$V_{te} \uparrow = \frac{(2V_{mp} \downarrow - V_{oc} \downarrow)(I_{sc} \downarrow - I_{mp} \downarrow)}{I_{mp} \downarrow - (I_{sc} \downarrow - I_{mp} \downarrow) \ln\left(\frac{I_{sc} \downarrow - I_{mp} \downarrow}{I_{sc} \downarrow}\right)}$$
 denominator is decreasing more than numerator

430 Similar results obtained for the estimated  $V_{te}$  in the column-level faulty PV conditions as shown in Fig  
 431 15(d). The main findings of this section can be listed as the following:

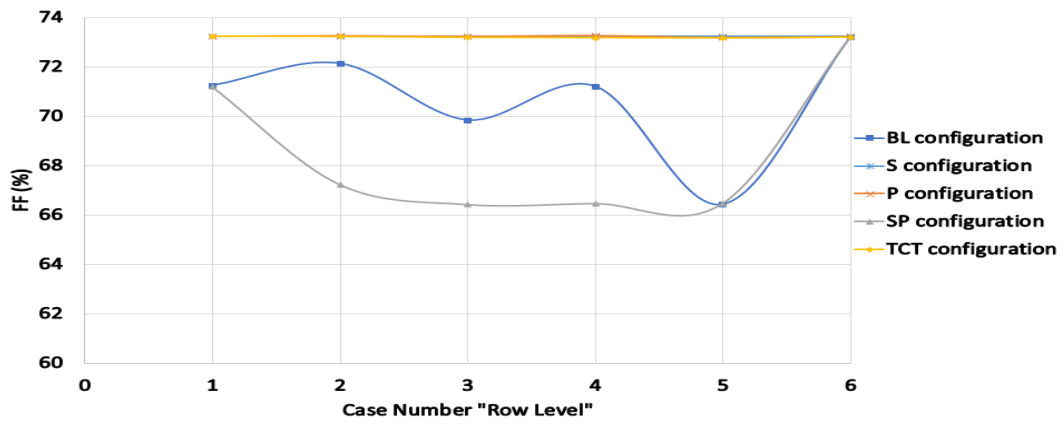
- 432 • When the number of faulty PV modules in increasing the estimated  $R_s$  is decreasing in S, SP TCT  
 433 and BL configurations.  
 434 • The FF for the S and P configurations among all faulty PV conditions remains at 73.2%.  
 435 • The estimated value of  $V_{te}$  for S, SP, TCT and BL configurations is decreased while increasing the  
 436 number of faulty PV modules. However, in case of the faulty PV string occurred in the PV system,  
 437 the value of the  $V_{te}$  is increased only in SP, TCT and BL configurations.  
 438 • P configuration has approximately constant levels of FF and  $V_{te}$  among all tested PV faulty  
 439 conditions.

Table 10  
 Estimated  $R_s$  for the Multiple Array Configurations, Scenario 3: PV Faulty Conditions, Row Level

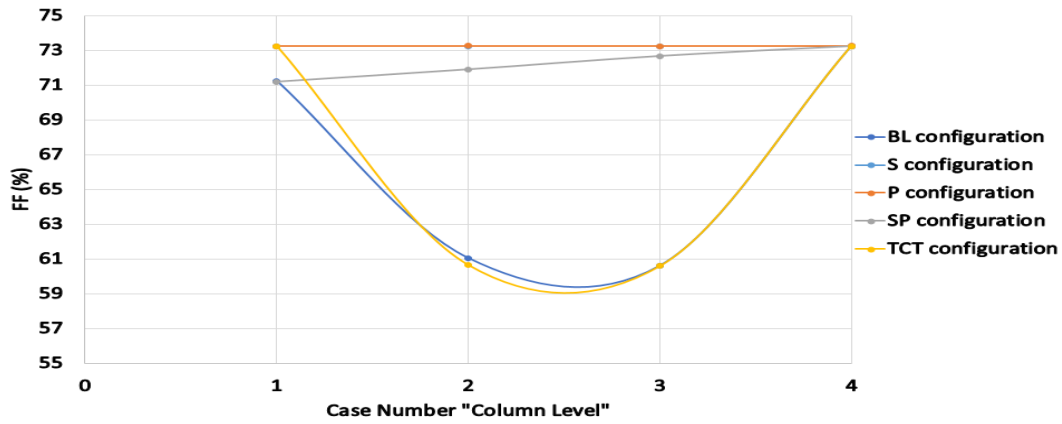
Case #	Estimated $R_s$ ( $\Omega$ )				
	S	P	SP	TCT	BL
Case 1	11.57273	0.022096	0.800641	0.631313	0.829876
Case 2	11.08033	0.023095	1.01688	0.505306	0.591541
Case 3	10.58574	0.024196	0.889442	0.379219	0.596659
Case 4	10.08065	0.025408	0.596659	0.253936	0.333778
Case 5	9.581603	0.026748	0.299043	0.128304	0.298151
Case 6	9.077156	0.028226	1.00776	1.00776	1.00776

Table 11  
 Estimated  $R_s$  for the Multiple Array Configurations, Scenario 3: PV Faulty Conditions, Column Level

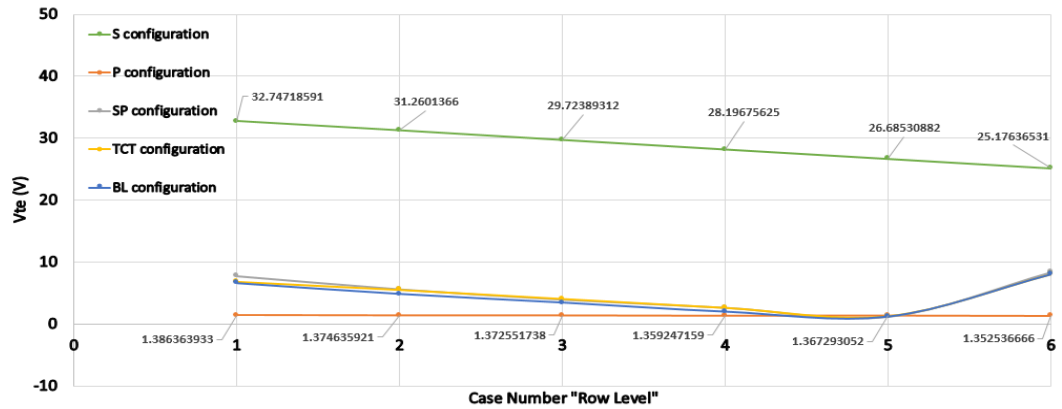
Case #	Estimated $R_s$ ( $\Omega$ )				
	S	P	SP	TCT	BL
Case 1	11.57273	0.022096	0.800641	0.631313	0.829876
Case 2	11.08033	0.023095	0.764526	0.884173	0.913242
Case 3	10.58574	0.024196	0.693481	1.135203	1.135203
Case 4	10.08065	0.025408	0.631313	0.631313	0.631313



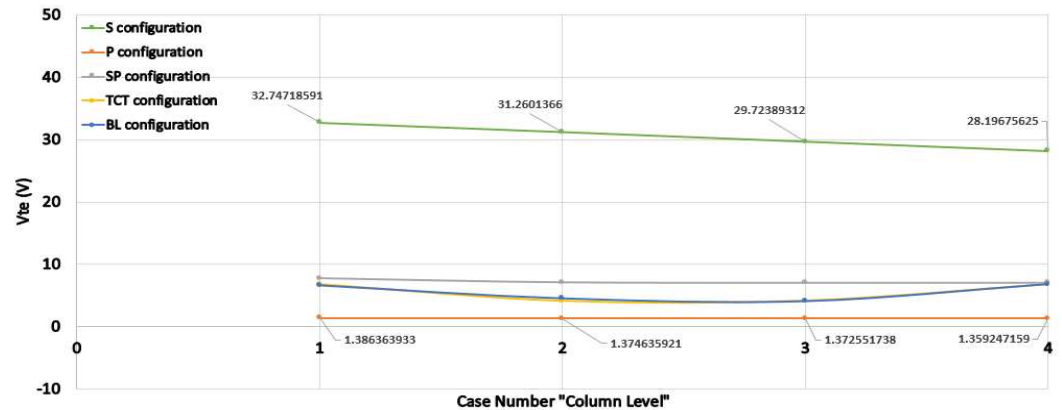
(a)



(b)



(c)



(d)

Fig. 15. FF and  $V_{te}$  Variations for Scenario 3: Faulty PV Conditions. (a) Fill Factor Variations for Row Level PV Faulty Conditions, (b) Fill Factor Variations for Column Level PV Faulty Conditions, (c)  $V_{te}$  Variations for Row Level PV Faulty Conditions, (d)  $V_{te}$  Variations for Column Level PV Faulty Conditions

441 5. *Discussion*

442 In this paper a brief modelling, simulation and data analysis of various partial shading and PV faulty  
443 modules conditions have been discussed. Multiple diagnostic indicators have been used to compare the  
444 performance of each PV array configuration such as short circuit current ( $I_{sc}$ ), current at maximum power  
445 point ( $I_{mpp}$ ), open circuit voltage ( $V_{oc}$ ), voltage at maximum power point ( $V_{mpp}$ ), series resistance ( $R_s$ ), fill  
446 factor (FF) and thermal voltage ( $V_{te}$ ). Few of these indicators have been demonstrated by F. Belhachat [6].

447 However, the partial shading conditions applied in this paper is not static as shown in [6, 7, 9 and 13], which  
448 means that the partial shading conditions are either increasing or decreasing among all PV modules.  
449 Additionally, in order to test the performance of each PV array configuration under faulty PV conditions,  
450 from 1 to 6 Faulty PV modules have been disconnected in order to compare between each PV indicator  
451 variations, this scenario has been demonstrated in section 4.3.3. Currently, there are few research articles  
452 which combines between faulty PV conditions with multiple PV array configurations. Therefore, this  
453 section is one of the major contribution for this paper.

454 The obtained results of this research can be divided into four main categories:

- 455 1. PV array configurations under standard test condition (STC):  
456 • The S, P, SP, TCT and BL configurations provide the same maximum output power.  
457 • FF for all PV array configurations is approximately equal to 73.2%.  
458 • New mathematical expressions have been derived for estimating the value of the series  
459 resistance  $R_s$  across one PV module in all tested PV array configurations.  
460
- 461 2. PV array configurations under uniform partial shading conditions:  
462 • P configuration provides the maximum output power when one to five rows or/and one to  
463 four columns are completely shaded.  
464 • S, SP, TCT and BL configurations have an increase of the  $R_s$  while increase the uniform  
465 shading across the PV modules. While P configuration series resistance remains at the same  
466 value which is approximate to 0.02  $\Omega$ .  
467 • FF for the S, SP, TCT and BL configurations have a significant drop in its value while  
468 increasing the uniform partials shading condition applied to a row of PV modules.  
469 However, the P configuration FF remains at a threshold of 74%.  
470 • The value of  $V_{te}$  is not a proper indicator for predicting/estimating the change in the partial  
471 shading conditions for S, SP, TCT and BL since it does not change among all tested  
472 uniform partial shading conditions.  
473
- 474 3. PV array configurations under non-uniform partial shading conditions:  
475 • P configuration provides the maximum output power when one to five rows and/or one to  
476 four columns are completely shaded. Furthermore, TCT configuration provided the second  
477 optimum output power among all other PV array configurations.  
478 • S, SP, TCT and BL configurations have an increase of the  $R_s$  while increase the non-uniform  
479 shading across the PV modules. While P configuration series resistance remains at the same  
480 value which is approximate to 0.02  $\Omega$ .  
481 • SP, TCT and BL configurations proves that when the reduction in the irradiance is greater  
482 than 2900 W/m<sup>2</sup> the estimated value of  $V_{te}$  is always greater than  $V_{te}$  threshold. Moreover,  
483 S configuration shows that the value of the  $V_{te}$  is greater than  $V_{te}$  threshold if: Reduction  
484 in irradiance  $\geq$  6000 W/m<sup>2</sup>.



485 4. PV array configurations under faulty PV conditions:

- 486 • P configuration provides the maximum output power when one to five PV modules are  
 487 faulty in a row of PV modules and when one to four PV modules are disconnected from a  
 488 column of PV modules in the PV array configuration.  
 489 • The estimation of the  $R_s$  of a single PV module in the PV array configurations can be  
 490 calculated using the following mathematical expression:

$$\text{S configuration} \quad \frac{R_s \text{ (Obtained from the I-V Curve)}}{24_{(\text{total PV module in the PV array configuration})}}$$

$$\text{P configuration} \quad R_s \text{ (Obtained from the I-V Curve)} \times 24_{(\text{total PV module in the PV array configuration})}$$

$$\text{SP, TCT and BL configurations} \quad \frac{R_s \text{ (Obtained from the I-V Curve)} \times 4_{(\text{number of PV columns})}}{6_{(\text{number of PV modules in one PV row "PV String"})}}$$

- 491 • The estimated value of  $V_{te}$  for S, SP, TCT and BL configurations is decreased while  
 492 increasing the number of faulty PV modules. However, in case of faulty PV string occurred  
 493 in the PV system, the value of the  $V_{te}$  is increased only in SP, TCT and BL configurations.  
 494 • The FF for the S and P configurations among all faulty PV conditions remains at 73.2%.  
 495 However, for all other PV configurations the estimated value of the FF is either increasing  
 496 or decreasing.

497 From the obtained results, it is evident that the variations of  $I_{sc}$ ,  $I_{mpp}$ ,  $V_{oc}$ , and  $V_{mpp}$  are not shown. This is  
 498 because the value of these indicators have been widely discussed by many research articles such as [6, 7, 9  
 499 and 13]. However, all listed references does not include the increase or decrease of shading patterns among  
 500 all PV configurations, additionally, there are few of discussions about faulty PV modules in multiple PV  
 501 array configurations.

502 Table 12, 13 and 14 illustrates the variations for all indicators used in this article among all examined partial  
 503 shading and faulty PV conditions in the S, P, SP, TCT and BL PV array configurations. Three different  
 504 symbols are used to show whether the value of the indicator has an “↓” decrease, “↑” increase, “–” no  
 505 change in its value and ↓↑ decrease or increase in the value of the indicator. A brief discussion of the  
 506 indicators  $R_s$ , FF and  $V_{te}$  are is available in section 4.

507 The S, SP, TCT and BL configurations have always a reduction in the value of  $V_{oc}$  while increasing the  
 508 uniform, non-uniform shading conditions and increasing the number of faulty PV modules. The P  
 509 configuration has a reduction in the  $V_{oc}$  among all shading patterns, however,  $V_{oc}$  remains constant while  
 510 increasing or decreasing the number of faulty PV modules.

511 In most tested conditions, the value of the  $I_{sc}$  has no change for the S, SP, TCT and BL configurations. The  
 512 P configuration proves that the value of  $I_{sc}$  is always decreasing while increasing the uniform, non-uniform  
 513 shading conditions and increasing the number of faulty PV modules.

514 The voltage at maximum power point ( $V_{mpp}$ ) is not a proper indicator for estimating/predicting partial  
 515 shading conditions or/and faulty PV modules in the S, SP, TCT and BL configuration because in each tested  
 516 condition the value of  $V_{mpp}$  is either increased or decreased. However, this comment is not applicable for  
 517 the P configuration because the value of the  $V_{mpp}$  is always decreasing while increasing the partial shading  
 518 conditions applied to the PV plant.

- 519 The last indicator,  $I_{mpp}$  is a proper indicator to estimate/predict partial shading conditions in all examined  
520 PV array configurations since the value of the indicator is decreasing while increasing shading conditions.  
521 The value of  $I_{mpp}$  does not change while increasing/decreasing number of faulty PV modules in S, SP, TCT  
522 and BL configurations. However, it does change significantly for the P configuration.

Table 12  
Change in the Estimated Indicators on Each PV Array Configuration

Scenario	PV array configurations													
	S							P						
	$I_{sc}$	$I_{mpp}$	$V_{oc}$	$V_{mpp}$	$R_s$	FF	$V_{te}$	$I_{sc}$	$I_{mpp}$	$V_{oc}$	$V_{mpp}$	$R_s$	FF	$V_{te}$
Increasing uniform shading on PV row	-	↓	↓	↓↑	↑	↓	↓↑	↓	↓	↓	↓	-	-	-
Increasing non-uniform shading on PV row	-	↓	↓	↓↑	↑	↓	↓↑	↓	↓	↓	↓	-	-	-
Increasing uniform shading on PV column	-	↓	↓	↓↑	↑	↓↑	↓↑	↓	↓	↓	↓	-	-	-
Increasing non-uniform shading on PV column	-	↓	↓	↓↑	↑	↓	↓	↓	↓	↓	↓	-	-	-
Increasing faulty PV modules in PV row	-	-	↓	↓	↓	-	↓	↓	↓	-	-	↑	-	↓
Increasing faulty PV modules in PV column	-	-	↓	↓	↓	-	↓	↓	↓	-	-	↑	-	↓

Table 13  
Change in the Estimated Indicators on Each PV Array Configuration

Scenario	PV array configurations													
	SP							TCT						
	$I_{sc}$	$I_{mpp}$	$V_{oc}$	$V_{mpp}$	$R_s$	FF	$V_{te}$	$I_{sc}$	$I_{mpp}$	$V_{oc}$	$V_{mpp}$	$R_s$	FF	$V_{te}$
Increasing uniform shading on PV row	-	↓	↓	↓↑	↑	↓↑	↑	-	↓	↓	↓↑	↑	↓	↓↑
Increasing non-uniform shading on PV row	-	↓	↓	↓↑	↑	↓	↓↑	-	↓	↓	↓↑	↑	↓	↓↑
Increasing uniform shading on PV column	-	↓	↓	↓	↑	-	-	↓	↓	↓	↓↑	↑	-	-
Increasing non-uniform shading on PV column	-	↓	↓	↓	↑	↓	↓↑	↓	↓	↓	↓↑	↑	↓	↓↑
Increasing faulty PV modules in PV row	-	-	↓	↓	↓↑	↓	↓	-	-	↓	↓	↓	-	↓
Increasing faulty PV modules in PV column	-	-	↓	↓	↓	↑	↓	-	-	↓	↓	↓	↓	↓

Table 14  
Change in the Estimated Indicators on Each PV Array Configuration

Scenario	PV array configuration						
	BL						
	$I_{sc}$	$I_{mpp}$	$V_{oc}$	$V_{mpp}$	$R_s$	FF	$V_{te}$
Increasing uniform shading on PV row	-	↓	↓	↓↑	↑	↓	↓↑
Increasing non-uniform shading on PV row	-	↓	↓	↓↑	↑	↓	↓↑
Increasing uniform shading on PV column	↓	↓	↓	↓	↑	-	-
Increasing non-uniform shading on PV column	↓	↓	↓	↓↑	↑	↓	↓↑
Increasing faulty PV modules in PV row	-	-	↓	↓	↓	↓↑	↓
Increasing faulty PV modules in PV column	-	-	↓	↓	↓↑	↓	↓

523 **6. Conclusion**

524 In this paper, multiple PV array configurations including series (S), parallel (P), series-parallel (SP), total-  
525 cross-tied (TCT) and bridge-lined (BL) have been tested under various partial shading and faulty  
526 photovoltaic (PV) conditions. Several indicators such as short circuit current ( $I_{sc}$ ), current at maximum  
527 power point ( $I_{mpp}$ ), open circuit voltage ( $V_{oc}$ ), voltage at maximum power point ( $V_{mpp}$ ), series resistance  
528 ( $R_s$ ), fill factor (FF) and thermal voltage ( $V_{te}$ ) have been used to compare the obtained results from the  
529 partial shading and PV faulty conditions. MATLAB/Simulink software is used to perform the simulation  
530 and data analysis for each examined PV array configuration.

531 The variations for all indicators across all PV array configurations have been reported and compared briefly.  
532 Additionally, new mathematical expressions have been derived to estimate the value of the series resistance  
533 across a single PV module in each PV array configuration under standard test conditions (STC) and faulty  
534 PV modules.

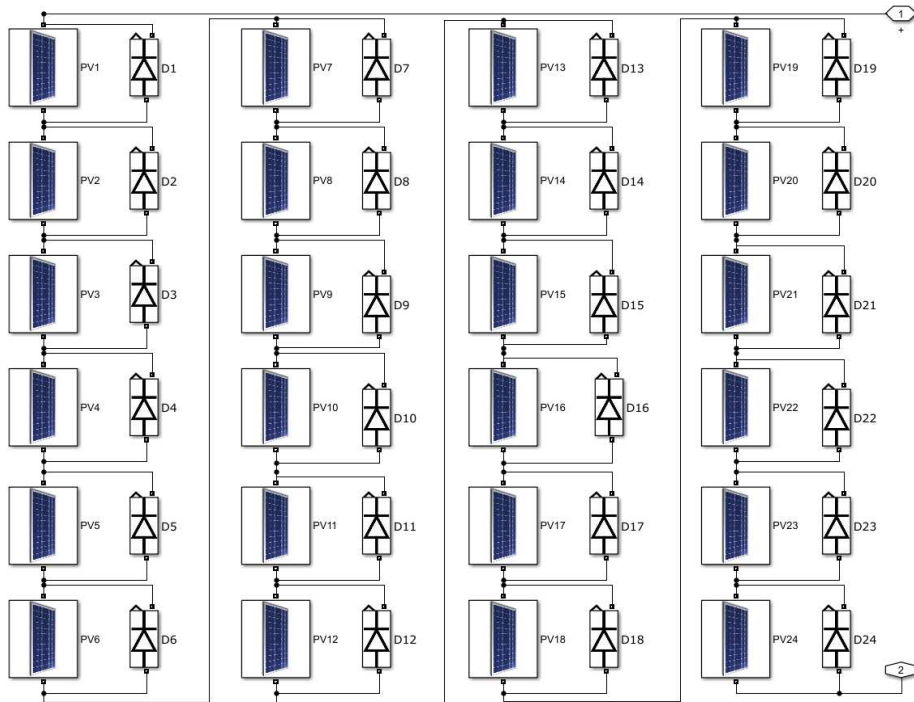
535 Finally, this study gives a useful information on the main parameters that could be used for  
536 estimating/predicting partial shading conditions in all examined PV array configurations. Therefore, the  
537 results obtained from this study could be enhanced by creating a generic algorithm using machine learning  
538 techniques for detecting faulty PV modules in multiple PV array configurations or/and creating a  
539 reconfigurable PV array system to improve the power generation in grid-connected PV (GCPV) plants.

540 **7. Acknowledgment**

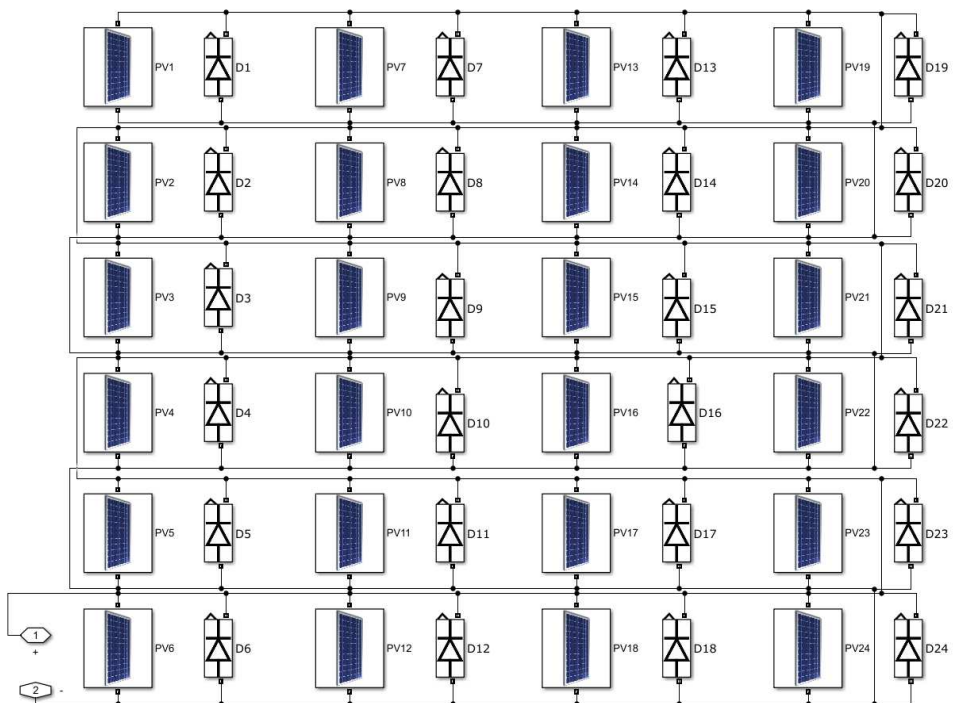
541 The authors would like to acknowledge the financial assistant to the University of Huddersfield,  
542 Engineering and Computing Department.

543 Appendix A. MATLAB/Simulink model for the examined PV array configurations.

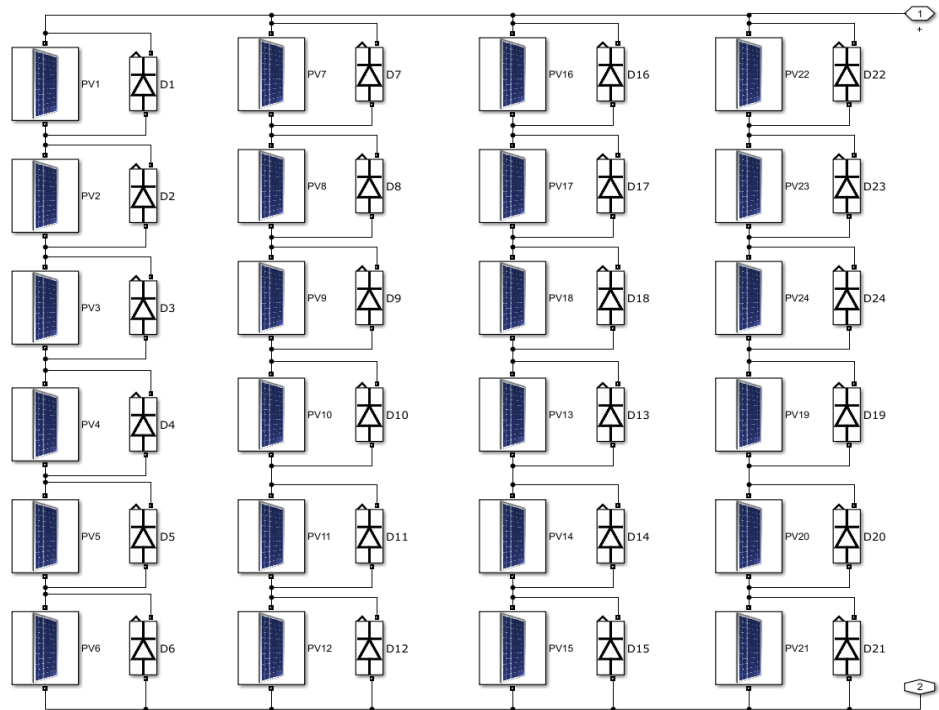
Series (S) Configuration:



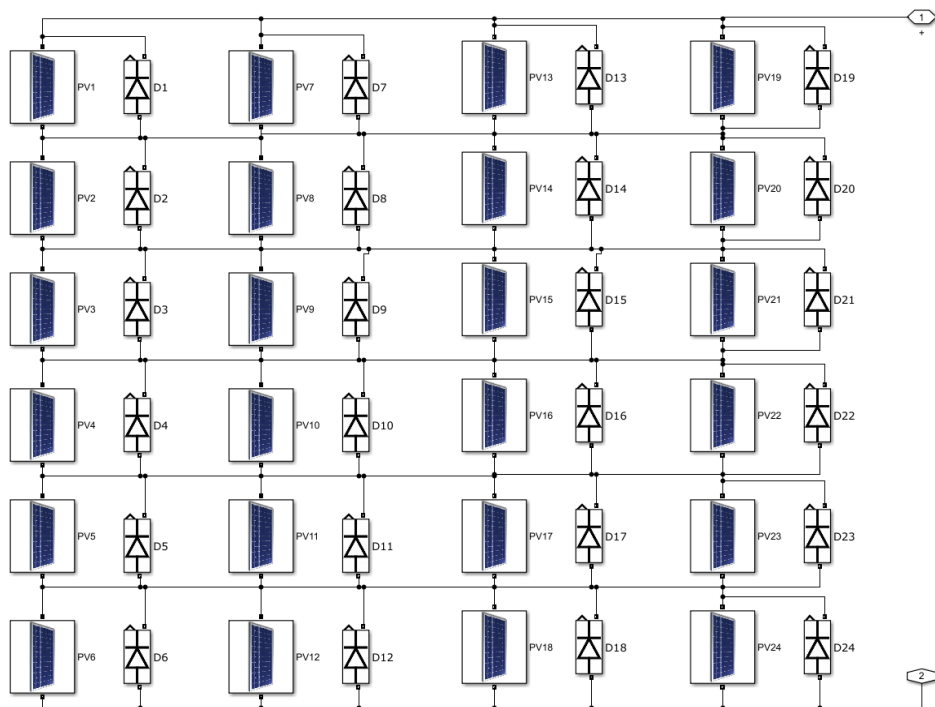
Parallel (P) Configuration:



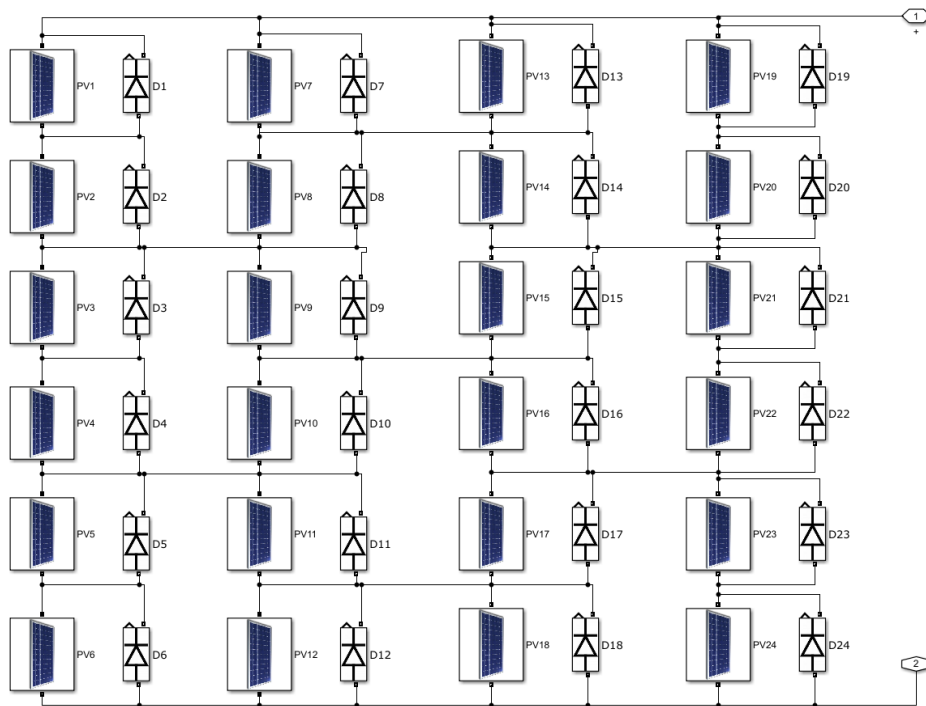
Series-Parallel (SP) Configuration:



Total-Cross-Tied (TCT) Configuration:



## Bridge-Linked (BL) Configuration:



## 544 References

- 545 [1] Makrides, G., Zinsser, B., Schubert, M., & Georghiou, G. E. (2014). Performance loss rate of twelve photovoltaic technologies  
546 under field conditions using statistical techniques. *Solar Energy*, 103, 28-42.
- 547 [2] Lappalainen, K., & Valkealahti, S. (2017). Output power variation of different PV array configurations during irradiance  
548 transitions caused by moving clouds. *Applied Energy*, 190, 902-910.
- 549 [3] Bai, J., Cao, Y., Hao, Y., Zhang, Z., Liu, S., & Cao, F. (2015). Characteristic output of PV systems under partial shading or  
550 mismatch conditions. *Solar Energy*, 112, 41-54.
- 551 [4] Di Vincenzo, M. C., & Infield, D. (2013). Detailed PV array model for non-uniform irradiance and its validation against  
552 experimental data. *Solar Energy*, 97, 314-331.
- 553 [5] Yeung, R. S. C., Chung, H. S. H., Tse, N. C. F., & Chuang, S. T. H. (2017). A global MPPT algorithm for existing PV system  
554 mitigating suboptimal operating conditions. *Solar Energy*, 141, 145-158.
- 555 [6] Belhachat, F., & Larbes, C. (2015). Modeling, analysis and comparison of solar photovoltaic array configurations under partial  
556 shading conditions. *Solar Energy*, 120, 399-418.
- 557 [7] Mohammadnejad, S., Khalafi, A., & Ahmadi, S. M. (2016). Mathematical analysis of total-cross-tied photovoltaic array under  
558 partial shading condition and its comparison with other configurations. *Solar Energy*, 133, 501-511.
- 559 [8] Wang, Y. J., & Hsu, P. C. (2011). An investigation on partial shading of PV modules with different connection configurations  
560 of PV cells. *Energy*, 36(5), 3069-3078.
- 561 [9] Ramaprabha, R., & Mathur, B. L. (2012). A comprehensive review and analysis of solar photovoltaic array configurations under  
562 partial shaded conditions. *International Journal of Photoenergy*, 2012.
- 563 [10] Ishaque, K., & Salam, Z. (2013). A review of maximum power point tracking techniques of PV system for uniform insolation  
564 and partial shading condition. *Renewable and Sustainable Energy Reviews*, 19, 475-488.
- 565 [11] Pareek, S., & Dahiya, R. (2016). Enhanced power generation of partial shaded photovoltaic fields by forecasting the  
566 interconnection of modules. *Energy*, 95, 561-572.
- 567 [12] Rani, B. I., Ilango, G. S., & Nagamani, C. (2013). Enhanced power generation from PV array under partial shading conditions  
568 by Shade dispersion using Su Do Ku configuration. *IEEE Transactions on sustainable energy*, 4(3), 594-601.

- 569 [13] Potnuru, S. R., Pattabiraman, D., Ganesan, S. I., & Chilakapati, N. (2015). Positioning of PV panels for reduction in line losses  
570 and mismatch losses in PV array. *Renewable Energy*, 78, 264-275.
- 571 [14] Chong, B. V. P., & Zhang, L. (2013). Controller design for integrated PV-converter modules under partial shading  
572 conditions. *Solar Energy*, 92, 123-138.
- 573 [15] Sun, D., Ge, B., Peng, F. Z., Haitham, A. R., Bi, D., & Liu, Y. (2012, May). A new grid-connected PV system based on  
574 cascaded H-bridge quasi-Z source inverter. In *Industrial Electronics (ISIE), 2012 IEEE International Symposium on* (pp. 951-956).  
575 IEEE.
- 576 [16] Koutroulis, E., & Blaabjerg, F. (2012). A new technique for tracking the global maximum power point of PV arrays operating  
577 under partial-shading conditions. *IEEE Journal of Photovoltaics*, 2(2), 184-190.
- 578 [17] Deshkar, S. N., Dhale, S. B., Mukherjee, J. S., Babu, T. S., & Rajasekar, N. (2015). Solar PV array reconfiguration under  
579 partial shading conditions for maximum power extraction using genetic algorithm. *Renewable and Sustainable Energy Reviews*, 43,  
580 102-110.
- 581 [18] Dhimish, M., & Holmes, V. (2016). Fault detection algorithm for grid-connected photovoltaic plants. *Solar Energy*, 137, 236-  
582 245.
- 583 [19] Dhimish, M., Holmes, V., & Dales, M. (2016, September). Grid-connected PV virtual instrument system (GCPV-VIS) for  
584 detecting photovoltaic failure. In *Environment Friendly Energies and Applications (EFEA), 2016 4th International Symposium*  
585 *on* (pp. 1-6). IEEE.
- 586 [20] Chine, W., Mellit, A., Pavan, A. M., & Kalogirou, S. A. (2014). Fault detection method for grid-connected photovoltaic  
587 plants. *Renewable Energy*, 66, 99-110.
- 588 [21] Chine, W., Mellit, A., Lughì, V., Malek, A., Sulligoi, G., & Pavan, A. M. (2016). A novel fault diagnosis technique for  
589 photovoltaic systems based on artificial neural networks. *Renewable Energy*, 90, 501-512.
- 590 [22] Silvestre, S., da Silva, M. A., Chouder, A., Guasch, D., & Karatepe, E. (2014). New procedure for fault detection in grid  
591 connected PV systems based on the evaluation of current and voltage indicators. *Energy Conversion and Management*, 86, 241-  
592 249.
- 593 [23] McEvoy, A., Castaner, L., & Markvart, T. (2012). *Solar cells: materials, manufacture and operation*. Academic Press.
- 594 [24] Sera, D., Teodorescu, R., & Rodriguez, P. (2007). PV panel model based on datasheet values. Paper presented at the 2392-  
595 2396. doi:10.1109/ISIE.2007.4374981
- 596 [25] Silvestre, S., Boronat, A., & Chouder, A. (2009). Study of bypass diodes configuration on PV modules. *Applied Energy*, 86(9),  
597 1632-1640.
- 598 [26] Sera, D., Teodorescu, R., & Rodriguez, P. (2008, November). Photovoltaic module diagnostics by series resistance monitoring  
599 and temperature and rated power estimation. In *Industrial Electronics, 2008. IECON 2008. 34th Annual Conference of IEEE* (pp.  
600 2195-2199). IEEE.
- 601 [27] Spataru, S., Sera, D., Kerekes, T., & Teodorescu, R. (2015). Diagnostic method for photovoltaic systems based on light I-V  
602 measurements. *Solar Energy*, 119, 29-44.
- 603 [28] Bastidas-Rodríguez, J. D., Franco, E., Petrone, G., Ramos-Paja, C. A., & Spagnuolo, G. (2015). Model-based degradation  
604 analysis of photovoltaic modules through series resistance estimation. *IEEE Transactions on Industrial Electronics*, 62(11), 7256-  
605 7265.
- 606 [29] Sera, D., Mathe, L., Kerekes, T., Teodorescu, R., & Rodriguez, P. (2011, November). A low-disturbance diagnostic function  
607 integrated in the PV arrays' MPPT algorithm. In *IECON 2011-37th Annual Conference on IEEE Industrial Electronics Society* (pp.  
608 2456-2460). IEEE.